eLIFE
24 Hills Road, P 01223 855346
Cambridge W elifesciences.org
CB2 1JP T @elife_sciences

FOR PEER REVIEW - CONFIDENTIAL

The Ret receptor regulates sensory neuron dendrite growth and integrin mediated adhesion

Tracking no: 04-11-2014-RA-eLife-05491R1

Peter Soba (University of Hamburg), Chun Han (Cornell University), Yi Zheng (Howard Hughes Medical Institute, University of California, San Francisco), Daniel Perea (Imperial College London), Irene Miguel-Aliaga (Imperial College London), Lily Yeh Jan (Howard Hughes Medical Institute, University of California, San Francisco), and Yuh Nung Jan (Howard Hughes Medical Institute, University of California, San Francisco)

Abstract:
Neurons develop highly stereotyped receptive fields by coordinated growth of their dendrites. Although cell surface cues play a major role in this process, few dendrite specific signals have been identified to date. We conducted an *in vivo* RNAi screen in *Drosophila* class IV dendritic arborization (C4da) neurons and identified the conserved Ret receptor, known to play a role in axon guidance, as an important regulator of dendrite development. The loss of *Ret* results in severe dendrite defects due to loss of extracellular matrix adhesion, thus impairing growth within a 2D plane. We provide evidence that *Ret* interacts with integrins to regulate dendrite adhesion via *rac1*. In addition, Ret is required for dendrite stability and normal F-actin distribution suggesting it has an essential role in dendrite maintenance. We propose novel functions for Ret as a regulator in dendrite patterning and adhesion distinct from its role in axon guidance.

Impact statement: Sensory neuron dendrite adhesion and stability requires Ret receptor function

Competing interests: No competing interests declared

Author contributions:
Peter Soba: ; Conception and design; Acquisition of data; Analysis and interpretation of data; Drafting or revising the article Chun Han: ; Analysis and interpretation of data; Drafting or revising the article; Contributed unpublished essential data or reagents Yi Zheng: ; Acquisition of data; Analysis and interpretation of data Daniel Perea: ; Drafting or revising the article; Contributed unpublished essential data or reagents Irene Miguel-Aliaga: ; Drafting or revising the article; Contributed unpublished essential data or reagents Lily Yeh Jan: ; Conception and design; Drafting or revising the article Yuh Nung Jan: ; Conception and design; Drafting or revising the article

Funding:
Lily Yeh Jan, Yuh Nung Jan The funders had no role in study design, data collection and interpretation, or the decision to submit the work for publication.

Datasets:
N/A

Ethics:
Human Subjects: No Animal Subjects: No

Author Affiliation:
Peter Soba(Center for Molecular Neurobiology, University Medical Campus,University of Hamburg,Germany;Department of Physiology,Howard Hughes Medical Institute,University of California,San Francisco,United States) Chun Han(The Weill Institute for Cell and Molecular Biology,Cornell University,United States;Department of Physiology,Howard Hughes Medical Institute,University of California,San Francisco,United States) Yi Zheng(Department of Physiology,Howard Hughes Medical Institute, University of California, San Francisco,United States;Department of Biochemistry and Biophysics,Howard Hughes Medical Institute,University of California,San Francisco,United States) Lily Yeh Jan(Department of Physiology,Howard Hughes Medical Institute, University of California, San Francisco,United States;Department of Biochemistry and Biophysics,Howard Hughes Medical Institute,University of California,San Francisco,United States) Yuh Nung Jan(Department of Physiology,Howard Hughes Medical Institute, University of California, San Francisco,United States;Department of Biochemistry and Biophysics,Howard Hughes Medical Institute,University of California,San Francisco,United States)

Dual-use research: No

Permissions: Have you reproduced or modified any part of an article that has been previously published or submitted to another journal? No

eLife Sciences Publications, Ltd is a limited liability non-profit nonstock corporation incorporated in the State of Delaware, USA with company number 5030732, and is registered in the UK with company number FC030576 and branch number BR015634 at the address 24 Hills Road, Cambridge, CB2 1JP.

eLife Sciences Publications, Ltd is a limited liability non-profit nonstock corporation incorporated in the State of Delaware, USA with company number 5030732, and is registered in the UK with company number FC030576 and branch number BR015634 at the address 24 Hills Road, Cambridge, CB2 1JP.

The Ret receptor regulates sensory neuron dendrite growth and integrin mediated adhesion

Peter Soba[1,2,5], Chun Han[2,3], Yi Zheng[2], Daniel Perea[4], Irene Miguel-Aliaga[4], Lily Yeh Jan[2], Yuh Nung Jan[2,5]

[1]Center for Molecular Neurobiology (ZMNH), University Medical Campus, University of Hamburg, Hamburg, Germany

[2]Howard Hughes Medical Institute, Departments of Physiology, Biochemistry and Biophysics, University of California, San Francisco, San Francisco, CA 94158, USA

[3]present address: The Weill Institute for Cell & Molecular Biology, Cornell University, Ithaca, USA

[4]Gut Signalling and Metabolism Group, MRC Clinical Sciences Centre, Imperial College London, UK

[5]to whom correspondence should be addressed: peter.soba@zmnh.uni-hamburg.de, yuhnung.jan@ucsf.edu

Abstract

Neurons develop highly stereotyped receptive fields by coordinated growth of their dendrites. Although cell surface cues play a major role in this process, few dendrite specific signals have been identified to date. We conducted an *in vivo* RNAi screen in *Drosophila* class IV dendritic arborization (C4da) neurons and identified the conserved Ret receptor, known to play a role in axon guidance, as an important regulator of dendrite development. The loss of *Ret* results in severe dendrite defects due to loss of extracellular matrix adhesion, thus impairing growth within a 2D plane. We provide evidence that *Ret* interacts with integrins to regulate dendrite adhesion via *rac1*. In addition, Ret is required for dendrite stability and normal F-actin distribution suggesting it has an essential role in dendrite maintenance. We propose novel functions for Ret as a regulator in dendrite patterning and adhesion distinct from its role in axon guidance.

Introduction

Accurate functional connectivity and sensory perception require proper development of the neuronal dendritic field, which ultimately determines the (sensory) input a specific neuron can receive and detect. Thus coordinated dendrite growth and patterning is important for establishing the often complex, but highly stereotyped organization of receptive fields. Two of the organizing principles in dendrite development are self-avoidance and tiling (Jan and Jan, 2010; Grueber and Sagasti, 2010; Zipursky and Sanes, 2010). While self-avoidance describes the phenomenon of recognition and repulsion of isoneuronal dendritic branches, tiling refers to the complete yet non-redundant coverage of a receptive field by neighboring neurons of the same type. Both phenomena have been described in different systems across species including the mouse, zebrafish, medicinal leech, *C. elegans* and *Drosophila melanogaster*.

Dendritic patterning by self-avoidance, tiling and other mechanisms is thought to be mediated by cell surface receptors and cell adhesion molecules (CAMs), which play a pivotal role in integrating environmental and cellular cues into appropriate growth and adhesion responses. Many such receptors, prominently Robo (Spitzweck et al., 2010) and Ephrin receptors (Egea and Klein, 2007), have well understood roles in axon guidance. Although some of these axonal cues including Robo/Slit play a role in dendrite development as well (Dimitrova et al., 2008; Gibson et al., 2014), dendritic surface receptors and their functions are not fully characterized to date. Recent efforts have yielded some progress in this area. *Down´s syndrome cell adhesion molecule* (*Dscam*) has been shown to regulate dendrite self-avoidance in *Drosophila* (Soba et al., 2007; Matthews et al., 2007; Hughes et al., 2007) and mouse (Fuerst et al., 2008, 2009). More recently, studies on protocadherins have revealed that they

play an important role in dendrite self-avoidance in mammals (Lefebvre et al., 2012). In *C. elegans*, sax-7/L1-CAM and menorin (mnr-1) form a defined pattern in the surrounding hypodermal tissue to guide PVD sensory neuron dendrite growth via the neuronal receptor dma-1 (Dong et al., 2013; Salzberg et al., 2013). However, given the complexity and stereotypy of dendritic arbors within individual neuronal subtypes, it is important to search for additional signals for directing dendrite growth.

The *Drosophila* peripheral nervous system (PNS) has served as an excellent model which has helped to elucidate several molecular mechanisms regulating dendrite development (Grueber and Sagasti, 2010; Jan and Jan, 2010). The larval PNS contains segmentally repeated dendritic arborization (da) neurons which have been classified as class I-IV according to their increasing dendritic complexity (Grueber et al., 2002). All da neuron classes feature highly stereotyped sensory dendrite projections. Moreover, isoneuronal dendrites of all da neurons exhibit self-avoidance behavior allowing them to develop their individual receptive fields without overlap. It has been demonstrated that all da neuron classes require *Dscam* for dendrite self-avoidance (Soba et al., 2007; Matthews et al., 2007; Hughes et al., 2007). In addition, the atypical cadherin *flamingo* (Matsubara et al., 2011) and immunoglobulin super family (IgSF) member *turtle* (Long et al., 2009) might play a more restricted role in C4da neuron self-avoidance. *Netrin* and its receptor *frazzled* have also been shown to act in parallel to *Dscam* in class III da neurons ensuring their proper dendritic field size and location by providing an attractive growth cue which is counterbalanced by self-avoidance (Matthews and Grueber, 2011). For tiling, no surface receptor has been identified to date. However, the conserved *hippo and tricornered* kinases, and more recently the *torc2* complex, have been implicated in C4da neuron tiling, as the loss of function of these genes results in iso- and

heteroneuronal crossing of dendrites (Emoto et al., 2004, 2006; Koike-Kumagai et al., 2009).

Recent work has further shown that dendrite substrate adhesion plays an essential role in patterning. Da neuron dendrites are normally confined to a 2D space through interaction with the epithelial cell layer and the extracellular matrix (ECM) on the basal side of the epidermis (Han et al., 2012; Kim et al., 2012; Yamamoto et al., 2006). 2D growth of da neuron dendrites requires integrins, as loss of the α-integrin *mew* (*multiple edomatous wing*) or ß-integrin *mys* (*myospheroid*) results in dendrites being freed from the 2D confinement due to detachment from the ECM. Thus they can avoid dendrites by growing into the epidermis leading to 3D crossing of iso- and hetero-neuronal branches (Han et al., 2012; Kim et al., 2012). Integrins are therefore essential to ensure repulsion-mediated self-avoidance and tiling mechanisms, which restrict growth of dendrites competing for the same territory (Han et al., 2012; Kim et al., 2012). How integrins are recruited to dendrite adhesion sites and whether they cooperate with other cell surface receptors is unknown.

To identify novel receptors required for generating complex, stereotypical dendritic fields, we performed an *in vivo* RNAi screen for cell surface molecules in C4da neurons. We identified the *Drosophila* homolog of *Ret* (*re*arranged *during transfection*) as a patterning receptor of C4da dendrites. Loss of *Ret* function in C4da neurons severely affects dendrite coverage, dynamics, growth and adhesion. In particular, dendrite stability and 2D growth are impaired resulting in reduced dendritic field coverage and abnormal 3D dendrite crossing, respectively. These defects can be completely rescued by Ret expression in C4da neurons. We further show that Ret interaction with integrins is needed to mediate C4da dendrite-ECM adhesion, but not dendrite growth. Our data suggest that *Ret* together with integrins acts through the

small GTPase *rac1*, which is required for dendrite adhesion and 2D growth of C4da neuron dendrites as well. We thus describe a novel role for the Ret receptor in dendrite development and adhesion by direct receptor crosstalk with integrins and its downstream signals.

Results

Expression analysis and RNAi-mediated knockdown of Ret reveal its role in C4da neuron dendrite development

To identify cell surface receptors mediating dendrite development of C4da neurons we used an *in vivo* RNAi screening approach. We focused on functionally defined classes of proteins containing conserved extracellular domains, including IgSFs and receptor tyrosine kinases (RTKs). To this end we expressed available RNAi transgenes specifically in the embryonic/larval PNS (*21-7-Gal4*) together with a C4da neuron-specific reporter line (*ppk*-CD4-tdTomato, Han et al., 2012). We also utilized a *UAS-Dcr2* transgene to enhance RNAi efficiency (Dietzl et al., 2007). Using this approach, we screened approximately 400 RNAi lines targeting IgSFs and RTKs and found that knockdown of Ret with two independent lines led to strong dendrite defects in C4da neurons (Figure 1 A). Knockdown of Ret resulted in abnormal C4da dendrite patterning with crossing of dendritic branches and incomplete coverage of their receptive field. We did not observe defects in other classes of da neurons (Figure 1-figure supplement 1 and data not shown) suggesting that Ret plays a specific role in C4da neuron dendrite morphogenesis.

Drosophila Ret encodes a highly conserved receptor tyrosine kinase (RTK) with neuronal expression (Hahn and Bishop, 2001; Kallijärvi et al., 2012; Sugaya et al.,

1994). In order to validate our RNAi results, we tested the expression of Ret in C4da neurons. A Gal4 enhancer trap line inserted within the 5'-region of the *Ret* gene showed C4da neuron expression when driving a GFP reporter (*UAS-CD8-GFP*, Figure 1 B). We next performed immunohistochemical analysis of larval filet preparations using Ret-specific antibodies. We first used a commercial phospho-Ret antibody which showed a mostly somatic granular signal only in C4da neurons (Figure 1-figure supplement 2 A). We tested its specificity with a mutant allele containing a P-element insertion within the 3'UTR region of the Ret gene (Ret^{C168}), which in combination with a deficiency covering the *Ret* locus ($Df(Bsc^{312})$) led to a strong reduction of the Ret immunoreactivity in C4da neurons (Figure 1-figure supplement 2 A-C). To validate and analyze Ret expression in C4da neurons in more detail, we raised a Ret specific antibody against its intracellular domain (see Material and Methods). Interestingly, Ret was detected throughout the dendritic arbor showing almost continuous staining along major dendrites (Figure 1 C,C') and a more granular pattern in terminal dendrites (Figure 1 C,C''). We detected granular Ret signal even in distal terminal dendrites suggesting that is localizing throughout the C4da dendritic arbor (Figure 1 D). In addition, the strongest Ret puncta consistently localized to the basal side of dendrites facing the ECM (Figure 1 C',C''). In *Ret* mutant animals, only residual immunoreactivity could be detected in C4da neuron somata but not in dendrites (Figure 1 E,E',F) suggesting that the allelic combination used is hypomorphic. Together, these results reveal expression and subtype specific functions of Ret in C4da neurons.

Loss of Ret function results in dendrite patterning and 3D crossing defects

We next wanted to corroborate the Ret-RNAi induced dendrite phenotype of C4da neurons using the Ret^{C168} allele. Compared to our RNAi results, we found very similar dendrite defects of C4da neurons in Ret^{C168} mutant animals (Figure 2 A,B). These defects were strongly enhanced when we combined Ret^{C168} with a chromosomal deficiency line ($Df(2L)Bsc^{312}$, Figure 2 C), indicating that Ret^{C168} is indeed a hypomorphic allele. Strikingly, *Ret* mutant C4da neurons displayed incomplete coverage of the receptive field, with dendritic terminals exhibiting patchy distribution, reflecting abnormalities in both shape and growth directionality. In addition, we observed severe isoneuronal dendrite crossing, resulting in extensive overlap of dendritic branches not normally observed in controls (Figure 2 B,C, arrows). This phenotype is reminiscent of self-avoidance defects described for *Dscam* (Hattori et al., 2009; Matthews et al., 2007; Soba et al., 2007) or tiling mutants like *trc, hpo and fry* (Emoto et al., 2004, 2006). To understand the nature of the dendritic crossing phenotype in *Ret* mutant larvae, we performed high resolution confocal live imaging of C4da neurons *in vivo*. Detailed 3D analysis of dendrite crossing points revealed that virtually all overlapping dendrites were not within the same focal plane, but grew in different planes without directly contacting one another (Figure 2 D,D',D''). Despite the severe patterning and field coverage defects, *Ret* mutant C4da neurons did not show a significant reduction in total dendrite length (Figure 2 E). They did however display excessive crossings of isoneuronal dendrites outside their normal 2D growth plane (Figure 2 F) and significantly reduced dendritic field coverage (see Figure 5 B,F). Taken together, our results show that *Ret* is required for C4da neuron dendrite patterning and field coverage, and *Ret* loss of function causes out of plane dendritic crossing due to abnormal 3D expansion of dendrites.

184

185 ***Ret loss of function results in ECM detachment and epithelial enclosure of***
186 ***C4da dendrites***

187 Due to the out of plane crossing observed in *Ret* mutant C4da neurons, we
188 suspected that dendrites were partially detached from the ECM and embedded within
189 the epithelial cell layer. A similar phenotype has recently been described for the
190 integrins *mew* and *mys,* which are required for dendrite-ECM adhesion in da neurons
191 (Han et al., 2012; Kim et al., 2012). In order to visualize C4da neuron dendrites and
192 the ECM, we took advantage of GFP protein traps for the ECM components *viking*
193 (vkg-GFP) and *trol* (trol-GFP) (Han et al., 2012). We performed two-color high
194 resolution confocal imaging of C4da neuron dendrites together with the GFP-labeled
195 ECM *in vivo*. In wildtype, the majority of dendrites were tightly interacting with the
196 ECM as previously reported (Figure 3 A, and Han et al., 2012). In *Ret* mutant
197 neurons however, large stretches of dendrites, in particular terminal arbors, were
198 detached from the ECM and enclosed by the epidermis (Figure 3 B). While
199 occasional detachment and out of plane crossing of dendrites could be observed in
200 controls (Figure 3 A'), the majority of branches were in tight proximity to the ECM
201 (Figure 3 A''). *Ret* mutant C4da neurons however displayed frequent detachment and
202 out of plane crossing of dendrites (Figure 3 B',B'') resulting in approx. 11% ECM-
203 detached dendrites within the dorsal field (Figure 3 C). Our results show that *Ret* is
204 required for robust dendrite-ECM interaction in C4da neurons.

205 To investigate a possible mechanistic link between dendrite-ECM adhesion defects in
206 *Ret* and *integrin* mutant C4da neurons, we next conducted genetic interaction
207 experiments. While animals heterozygous for *Ret* or *integrin* mutations showed no
208 significant dendrite detachment compared to wildtype, trans-heterozygous

combinations of *Ret* and *mys* or *mew* integrin alleles resulted in a significant increase in dendrite crossing defects (not shown) and a substantial loss of dendrite-ECM interaction (Figure 3 D-H). Similarly to *Ret* mutant C4da neurons, about 10% of dendrites were detached from the ECM in Ret^{C168}/mew^{M6} and Ret^{C168}/mys^{1} trans-heterozygous animals (Figure 3 I). These results suggest that *Ret* and integrins act in the same genetic pathway to promote dendrite-matrix interactions.

Ret is a cell surface protein and interacts with integrins in dendrites

To further assess the link between Ret and integrins we examined the cellular localization and interaction of Ret with Mys and Mew. We first performed immunohistochemical analysis of larval filet preparations co-expressing Ret together with Mys and Mew in C4da neurons, as integrins endogenous to C4da neurons are difficult to detect due to strong expression in the surrounding epithelial cells (Han et al., 2012). To this end, we used a mCherry-tagged Ret transgene which showed a distribution in dendrites similar to endogenous Ret and did not cause obvious phenotypes (Figure 4-figure supplement 1 A). We found partial co-localization of Ret and Mew or Mys in punctate structures in C4da neuron dendrites (Figure 4-figure supplement 2 and 3). Co-localized punctae of Ret and integrins could readily be detected in both primary and high order dendritic branches of C4da neurons (Figure 4-figure supplement 2 A',A'', 3 A',A''). Consistently, transfected S2 cells also displayed co-localization of Ret and Mys, particularly in filopodia-like structures close to the cell surface (Figure 4-figure supplement 1 B) suggesting that Ret and integrins may form a molecular complex. We therefore performed co-immunoprecipitation experiments of Ret and Mys/Mew in S2 cells. Indeed, Ret showed strong and specific interaction with Mys, and additional co-expression of Mew robustly increased the Ret-

integrin interaction indicating that Ret preferentially interacts with the mature integrin complex (Figure 4-figure supplement 1 C).

To investigate if Ret can also localize to the surface of C4da dendrites and possibly interact with adhesion mediating integrin complexes, we used a tagged Ret transgene carrying an N-terminal pHluorin in addition to the C-terminal mCherry-tag. We performed cell-surface immunostainings of Ret using an anti-GFP antibody recognizing the pHluorin-tag together with Mew immunostaining to assess its localization and co-distribution. Ret itself displayed pronounced surface labeling along the entire dendritic tree, strongly indicating that Ret is present at the cell surface of C4da neurons (Figure 4 A,B). Overall, the pHluorin signal showed a very surface Ret labeling throughout the dendritic arbor, while the intracellular mCherry-tag revealed additional punctate structures likely reflecting intracellular vesicles (Figure 4 A). Strikingly, Ret showed significant co-localization with Mew in dendrites (Figure 4 B). Intensity plots of Ret and Mew signals display a high degree of co-distribution in low and high order dendrites (Figure 4 B',B''). In particular, many of the high intensity peaks of Mew showed concomitant Ret signal peaks with both tags indicating that Mew and Ret can be indeed co-localized in dendrites and at the surface of C4da neurons. Quantitative colocalization analysis of Ret and integrin signals in C4da neuron somata and dendrites revealed a strong positive correlation based on Pearson coefficient analysis for overexpressed Ret/Mew and Ret/Mys (Figure 4 C).

Finally, we assessed colocalization of endogenous Ret with overexpressed integrins. As for Ret overexpression, endogenous Ret displayed a significant degree of co-distribution with Mys and Mew in C4da neurons (Figure 4 D,E). Besides pronounced colocalization in the C4da soma, patches of Ret/Mys and Ret/Mew punctae were

detected throughout the dendritic arbor in high (Figure 4 D',E') and low order branches (Figure 4 D'',E''). Interestingly, the majority of co-localized signals were found facing the basal dendritic surface which contacts the ECM (Figure 4 D',E', arrows and Video 1) suggesting that Ret and integrins are potentially interacting at adhesion sites. Overall, quantitative colocalization analysis of endogenous Ret and integrins showed positively correlated Pearson coefficients (Figure 4 F) suggesting that a subset of Ret and integrins are associated in C4da neurons.

Our genetic and immunohistochemical data therefore support the molecular interaction between Ret and integrins in C4da dendrites. These findings further suggest that Ret and integrins are forming a common pathway required for normal dendrite growth and ECM adhesion.

Ret or integrin overexpression in C4da neurons rescues Ret mutant dendrite adhesion defects

Although the Ret RNAi results and its expression pattern (see Figure 1) indicated a cell-autonomous function of *Ret*, we wanted to test its sufficiency for supporting normal C4da neuron dendrite morphology. Due to the close proximity of the *Ret* gene to the chromosomal centromere it was not possible to conduct MARCM analysis (mosaic analysis with a repressible cellular marker (Lee and Luo, 1999). Instead, we performed a rescue experiment by specifically expressing a mCherry-tagged Ret transgene in C4da neurons in the *Ret* mutant background. Indeed, driving expression of Ret in C4da neurons was sufficient to completely rescue the dendrite growth and crossing phenotype (Figure 5 B,B' and Figure 5 C,C') demonstrating that *Ret* is cell-autonomously required for C4da dendrite patterning.

We also asked if overexpression of the α/β-integrin complex is able to rescue dendrite-ECM interactions in *Ret* mutant animals. To this end, we overexpressed Mys and Mew in *Ret* mutant C4da neurons and assessed dendritic crossing and field coverage. Although the overexpression of integrins did not rescue all aspects of the Ret dendritic growth phenotype (Figure 5 D,D'), it completely prevented dendritic out of plane crossing indicating restored interaction with the ECM (Figure 5 E). However, unlike Ret itself, integrin overexpression in C4da neurons did not rescue coverage defects of the dendritic field in *Ret* mutant animals (Figure 5 F). Co-overexpression of Mys and Mew alone did not cause dendrite abnormalities (data not shown and Han et al., 2012) indicating that *Ret* dependent growth involves both integrin dependent and integrin independent pathways. Interestingly, Ret overexpression in the compound eye has been reported to cause photoreceptor degeneration (Read et al., 2005). We thus tested if co-expression of integrins could modulate Ret neurotoxicity in photoreceptor neurons (Figure 5-figure supplement 1). Integrin over-expression itself did not cause any eye phenotype, but was able to completely suppress Ret dependent photoreceptor degeneration. These findings show that, similarly to their interactions in C4da neurons, Ret and integrins genetically and functionally interact in the eye.

Our data provide evidence that Ret and the integrins *mys* and *mew* likely operate together in a common pathway to regulate dendrite adhesion to the ECM.

Rac1 loss of function causes loss of dendrite ECM adhesion and rac1 genetically interacts with Ret and integrins

In order to gain insight into the underlying intracellular signals we investigated candidate pathways common to RTK and integrin signaling. Rho family GTPases, particularly rac1, have been implicated in actin dynamics and dendrite morphogenesis of sensory neurons (Lee et al., 2003) and are a common target of both RTK and integrin signaling in many systems (reviewed in Ivaska and Heino, 2011). Using loss of function analysis we tested whether *rac1* is involved in dendrite ECM adhesion of C4da neurons. Loss of *rac1* function led to strong dendrite-ECM detachment and epithelial enclosure of dendrites highly similar to Ret and integrin mutant phenotypes (Figure 6A-C). Overall, in *rac1* mutant C4da neurons, 15% of dendrites in the field were detached from the ECM, an effect that was even more pronounced when the gene dosage of the other two rac-like GTPases, *rac2* and *mtl* was also reduced (Figure 6 C,D). In both cases, loss of *rac1* function also led to many non-contacting crossing defects of dendritic branches (Figure 6 B,C arrows, and Figure 6 E) indicating that self-avoidance is impaired due to 3D growth of dendrites lacking *rac1* function.

We next tested whether *Ret* and integrins are in the same genetic pathway as *rac1* by analyzing heterozygous allelic combinations. Animals heterozygous for *Ret*, *integrins* or *rac1* did not show significant changes in C4da neuron dendrite-ECM adhesion compared to wildtype (Figure 6 F-I). When combining *rac1* alleles with *Ret* or *integrin* mutant alleles however, we observed strong enhancement of dendritic loss of ECM adhesion (Figure 6 J-L). For both *Ret/rac1* and *integrin/rac1* heteroallelic combinations, 15-20% percent of dendrites lost contact with the ECM indicating strong crosstalk and regulation of Ret and integrins via rac1. These findings strongly suggest that *rac1* functions in the same pathway as *Ret* and integrins in regulating the attachment of dendrites to the ECM.

Ret mutant C4da neurons display increased dendrite turnover and abnormal F-actin localization

Unlike *Ret*, neither integrin nor *rac1* loss of function resulted in major defects in dendrite growth and coverage of C4da neurons. In addition, integrin overexpression was not able to rescue *Ret* dependent dendrite coverage defects (see Figure 5). We reasoned that Ret likely exerts additional functions independent of integrins/rac1. We thus investigated the specific effects of Ret on dendrite growth and turnover. To this end, we performed time lapse analysis during late larval development at 72h and 96h after egg laying (AEL). This allowed us to monitor dendrite dynamics within a 24h period. In wildtype C4da neurons, significant turnover of terminal dendrites could be observed (Figure 7 A), as reported previously (Parrish et al., 2007). Overall, we detected dendrite growth and terminal dynamics required to maintain overall field coverage and tiling during larval growth. In *Ret* mutant animals however, C4da neuron dendrites already showed defects at 48h AEL (not shown) and 72h AEL, as evident from incomplete coverage and abnormal dendrite patterning at that stage (Figure 7 B). Increased dendrite crossing was also already apparent. Remarkably, analysis of dendrite turnover between 72-96h AEL revealed highly increased dynamics of dendritic growth and retraction, with major remodeling of the terminal dendrite arbors. Both growth and retraction of dendrite terminals in *Ret* mutant C4da neurons was increased two to three-fold compared to wildtype (Figure 7 C). Overall, the growth/retraction ratio of dendrites was significantly reduced in *Ret* mutant C4da neurons due to a disproportional increase in retraction compared to growth (Figure 7 D). Our findings therefore suggest that Ret function is important for stabilizing growing dendrites.

We suspected that the observed increase of dendrite dynamics in *Ret* mutant C4da neurons was linked to the actin cytoskeleton, as integrins, Rac1 as well as Ret are able to directly or indirectly regulate actin (Fukuda et al., 2002). To investigate this possibility, we used LifeAct imaging (Riedl et al., 2008) to analyze F-actin distribution in dendrites *in vivo*. Wildtype C4da neurons displayed fairly even distribution of F-actin along major dendrites, while terminal branches typically featured hotspots of increased F-actin levels (Figure 7 E,F). In contrast, F-actin levels were significantly increased and unevenly distributed in proximal regions of primary dendrites of *Ret* mutant neurons (Figure 7 E, G). The increase in proximal F-actin leveled out at more distal parts of the primary branches, where it reached similar levels in both genotypes (Figure 7 E). The overall F-actin distribution in major branches of *Ret* mutant C4da neurons was significantly different from wildtype ($p<0.05$, $n=5$). Strikingly, aberrantly crossing terminal branches had increased levels of F-actin, while other terminals displayed either normal or very low F-actin levels compared to wildtype (Figure 7 G, arrows). This was also reflected in the centralization and overall uneven distribution of F-actin along dendritic arbors due to the lack of *Ret* function (Figure 7 E). This data clearly shows that Ret is required for the appropriate localization of F-actin in dendrites, which likely contributes to the destabilization of growing branches.

Taken together, our findings show that loss of *Ret* function impairs dendrite stability and increases dynamic growth and retraction of dendritic branches resulting in the failure of complete receptive field coverage. This is likely linked to the observed abnormal distribution of F-actin in the absence of *Ret*, which indicates a lack of appropriate growth signals and abnormal activity of the underlying signaling machinery coordinating actin dynamics.

Discussion

In this study, we provide evidence that Ret is a regulator of dendrite growth and patterning of C4da sensory da neurons. *Ret* is a conserved receptor tyrosine kinase (RTK) expressed in the nervous system of vertebrates (Pachnis et al., 1993; Schuchardt et al., 1994) and *Drosophila melanogaster* (Hahn and Bishop, 2001; Sugaya et al., 1994), and has been shown to have a number of important functions in nervous system development and maintenance: it regulates motor neuron axon guidance (Kramer et al., 2006), dopaminergic neuron maintenance and regeneration (Kowsky et al., 2007; Kramer et al., 2007), and mechanoreceptor differentiation and projection to the spinal cord and medulla (Bourane et al., 2009; Luo et al., 2009). Ret signaling is activated by binding to glial cell line derived neurotrophic factor (GDNF) family ligands and their high affinity co-receptors, the GDNF family receptors (GFRα) (reviewed in Runeberg-Roos and Saarma, 2007). Ret also plays an important role in human development and disease as loss of function mutations of Ret lead to Hirschprung's disease displaying colonic aganglionosis due to defective enteric nervous system development (Amiel et al., 2008). Conversely, Ret gain of function mutations are causal for autosomal dominant MEN2 (multiple endocrine neoplasia type 2) type medullary thyroid carcinoma (Almeida and Hoff, 2012; Lairmore et al., 1993).

Prior to this study, Ret has not been implicated in dendrite development. Here, we show that Ret is required specifically for 2D growth of C4da neurons by regulating integrin dependent dendrite-ECM adhesion. Normally, C4da neuron dendrites are virtually always in contact with the ECM and the basal surface of the epithelium lining the larval cuticle, and thus tightly sandwiched between the two compartments (Han et al., 2012; Kim et al., 2012; Yamamoto et al., 2006). In both integrin and *Ret* mutants,

406 dendrite-ECM adhesion is impaired. Ret and integrins can co-localize in dendrites
407 and thus likely form a functional complex that could induce and maintain adhesion of
408 dendrites to the ECM. Since *Ret* loss of function primarily leads to detached terminal
409 dendrite branches, it is tempting to speculate that Ret might be required to recruit
410 integrins to sites of growing dendrites to promote ECM interaction. This is supported
411 by the co-localization of Ret and integrins on the dendrite surface. Their cooperative
412 interaction could thus ensure proper adhesion of growing branches and, conversely,
413 the fidelity of self-avoidance and tiling.

414 Our results also highlight the importance of integrating different guidance and
415 adhesion cues to achieve precise neuronal patterning. This has so far only been
416 studied in axon guidance *in vivo* (Dudanova and Klein, 2013). Interestingly,
417 vertebrate *Ret* has been shown to cooperate with Ephrins to ensure high fidelity axon
418 guidance in motor neurons by mediating attractive EphrinA reverse signaling
419 (Bonanomi et al., 2012; Kramer et al., 2006). Similar mechanisms may conceivably
420 be employed for growing dendrites, which also encounter a multitude of attractive,
421 repulsive and adhesive cues that have to be properly integrated. Besides pathways
422 acting independently or in a parallel fashion, an emerging view is that receptors
423 exhibit direct crosstalk to integrate incoming signals. So far, only parallel receptor
424 pathways like Dscam and Netrin-Frazzled signaling in class III da neurons (Matthews
425 and Grueber, 2011) or Dscam/integrins (Han et al., 2011; Kim et al., 2012) have been
426 identified co-regulating dendrite morphogenesis. Our data from this study shows that
427 the Ret receptor and integrins integrate dendrite adhesion and growth by
428 collaborative interaction of the two cell surface receptors. The molecular and genetic
429 link between *Ret* and integrins suggests that in this case direct receptor crosstalk
430 plays a major role in their function. How exactly these cell surface receptors

cooperate and interact remains to be elucidated. Integrins have been shown to display extensive crosstalk with other signaling receptors, including RTKs (Ivaska and Heino, 2011). Although integrins are involved in adhesion of virtually all cell types, the underlying signaling and recruitment of integrins to sites of adhesion *in vivo* is complex and not completely understood. It has been suggested that integrin and growth factor receptor crosstalk can occur by concomitant signaling, collaborative activation, or direct activation of associated signaling pathways (Ivaska and Heino, 2011). For example, matrix-bound VEGF can induce complex formation between VEGFR2 and β1-integrin with concomitant targeting of β1-integrin to focal adhesions in endothelial cells (Chen et al., 2010). Our findings of biochemical interaction and co-localization of Ret with the α/β-integrins *mys* and *mew* in C4da neuron dendrites argue in favor of direct receptor interaction and subsequent activation of a common signaling pathway.

Integrins and RTKs like Ret do share some of the same intracellular signaling components. These comprise, among others, the MAPK (mitogen-activated protein kinase) pathway, Pi3-Kinase (Pi3K), and Rho family GTPases including Rac1 (Ivaska and Heino, 2011). Previous studies provide evidence for Ret-integrin-Rac1 interplay *in vitro* showing that Ret can enhance integrin mediated adhesion (Cockburn et al., 2010) and induce Rac1 dependent lamellipodia formation (Fukuda et al., 2002) in cell culture models. In primary chick motor neurons, Rac1 is involved in neurite outgrowth on the integrin substrates laminin and fibronectin (Kuhn et al., 1998). Interestingly, Rac1 has previously been shown to regulate dendrite branching in C4da neurons (Emoto et al., 2004; Lee et al., 2003), however a role in dendrite adhesion *in vivo* has not been described before. In our study we show that Rac1 is required for dendrite-ECM adhesion similarly to what has been described for integrins and we genetically

link Ret and integrin dependent adhesion with Rac1 function. In *Drosophila*, MAPK, Src and PI3K can be activated by constitutively active Ret overexpression in the compound eye (Dar et al., 2012; Read et al., 2005). Moreover, novel inhibitors of Ret signaling targeting Raf, Src and S6-Kinase (S6K) prevent lethality induced by Ret over-activation in a *Drosophila* multiple endocrine neoplasia (MEN2) model (Dar et al., 2012). Interestingly, S6K has been shown to be involved in dendrite growth but not tiling in C4da neurons (Koike-Kumagai et al., 2009). It remains to be shown if these pathways play a direct role in *Ret* function in dendrite adhesion and growth.

Notwithstanding important commonalities, *Ret* function in C4da neurons cannot be fully explained by crosstalk with integrins and *rac1*. Reduced dendritic field coverage, likely due to the observed increase in dendrite turnover, is only evident in *Ret* but not in integrin or *rac1* mutant C4da neurons. Moreover, increasing integrin expression in a *Ret* mutant background did not rescue dendrite coverage defects, albeit it prevented dendrite crossing. These findings indicate that Ret has additional functions in dendritic branch growth and stability that require as yet unknown extracellular and intracellular mediators. This is also supported by the aberrant F-actin localization in neurons lacking Ret. Here, Ret dependent intracellular effectors are likely important for F-actin assembly to support directed dendrite growth and stabilization, and their localization and activity might be deregulated in the absence of Ret.

Drosophila Ret is a highly conserved molecule, its cognate vertebrate ligand GDNF, however is not (Airaksinen et al., 2006). In addition, *Drosophila* Ret can neither bind GDNF nor transduce GDNF signaling, although it has been shown to contain a functional tyrosine kinase domain (Abrescia et al., 2005). In mammals, the GFRα co-receptors are essential components of GDNF/Ret signaling (Runeberg-Roos and Saarma, 2007). A *Drosophila* GFR-like homolog (dGFRL) has recently been

characterized and was found to function and interact with the NCAM homolog FasII (Kallijärvi et al., 2012). Therefore, it appears that Ret's functional interaction partners in dendrite development differ significantly from the previously described co-factors in other systems. It is interesting to speculate that a yet undiscovered Ret ligand is involved in Ret mediated dendrite growth and branch stabilization, which might have implications for mammalian Ret function as well: due to its role in the maintenance of dopaminergic neurons and motor axon growth in mouse (Kramer et al., 2006, 2007), adhesion related signaling via integrins could well be important during these processes. Moreover, the formation of a dorsal root ganglia derived mechanosensory neurons and their afferent and efferent fiber growth and innervation depends on Ret expression (Bourane et al., 2009; Luo et al., 2009). It will be interesting to investigate the functional interplay of Ret and integrins in central and peripheral target innervation and neurite maintenance in these systems, given the interdependent function of *Ret* and integrins in sensory dendrite growth as shown in our study.

In summary, we describe a novel role for the Ret receptor in dendrite branch growth and stability in *Drosophila* C4da neurons. This role involves cell-autonomous effects of Ret on ECM adhesion, and F-actin localization in these neurons. Moreover, we have linked dendritic adhesion defects attributable to *Ret* to integrin and *rac1* function featuring a novel and possibly conserved mode of action for Ret in dendrite development.

Experimental Procedures

Fly stocks and transgenic constructs

All fly stocks were maintained at 25°C and 70% rel. humidity on standard cornmeal/molasses food. The following fly stocks were used: Ret^{C168}, Ret^{NP7645}, mys^{1},mew^{M6}, $rac1^{J11}$, $rac1^{J10}rac2^{\Delta}mtl^{\Delta}$ (Hakeda-Suzuki et al., 2002; Ng et al., 2002), *ppk-CD4-tdTomato, ppk-Gal4, UAS-CD4-tdGFP* (Han et al., 2012), *trol-GFP, vkg-GFP, UAS-LifeAct-mCherry* (kindly provided by J. Wildonger).

Ret^{C168} is a Piggyback transposon insertion in the 3´UTR of *Ret* and likely a hypomorphic allele leading to reduced Ret protein expression. $Df(2L)Bsc^{312}$ is a deficiency covering the genomic *Ret* locus.

Ret cDNA was amplified from pGMR-Ret (kind gift from Ross Cagan) and cloned into pUAST-attB (Groth et al., 2004). In addition, we generated Ret constructs carrying a C-terminal mCherry tag or an additional pHluorin-tag inserted downstream of the 5' signal peptide sequence.

UAS-LifeAct-mCherry, UAS-Ret and UAS-Ret-mCherry, UAS-pHluorin-Ret-mCherry transgenes were generated by embryo injection into *vasa-ΦC31;attP*^{2} carrying flies according to standard procedures (Groth et al., 2004). The *ΦC31*-integrase was outcrossed and transgenes were combined with the appropriate alleles and markers.

Anti-Ret antibody generation

An antibody against the Ret receptor was generated in guinea pigs by co-injecting the synthetic peptides ETKEVSPGWQAEDAV (peptide 1, corresponding to amino acids 1221-1235 of the intracellular C terminus) and DIHDQATSYDQSEEEM

(peptide 2, corresponding to amino acids 1095-1110 of the intracellular C terminus). The resulting antiserum was affinity purified against peptide 1 and used at a 1:1000 dilution. Peptide synthesis, antibody generation, and affinity purification were outsourced to Eurogentec.

Immunohistochemistry and antibodies

Larval filet preparation and staining was essentially performed as described (Han et al., 2012). The following antibodies were used: rabbit anti-phospho-Ret (1:50, Cell Signaling Technology, Danvers, MA), mouse anti-GFP (1:100, Roche Diagnostics, Mannheim, Germany), mouse anti-mys (1:200, Developmental Studies Hybridoma Bank, (DSHB), Iowa City, IO), mouse anti-mew (1:50, DSHB). Secondary DyLight or Alexa conjugated donkey antibodies were from Jackson ImmunoResearch (Westgrove, PA) and were used at 1:400-1:1000.

Quantitative immunohistochemistry of Ret

Larval filets of wildtype or *Ret* mutant animals carrying a C4da neuron specific marker (*ppk-Gal4>CD4-tdGFP*) were prepared and immunostained as described above with rabbit anti-phospho-Ret (1:50, Cell Signaling Technology, Danvers, MA) or guinea pig anti-Ret (1:1000) antibodies. We quantified the Ret antibody signal of C4da neuron somata in confocal image stacks and calculated signal over background ratios ($\Delta F/F$) by subtracting averaged background signal flanking the C4da soma region (F). Statistical significance for the two genotypes was calculated using a two-tailed *t*-test.

551

552 *Cell surface immunostaining of pHluorin-tagged Ret*

553 For cell surface staining of pHluorin-Ret-mCherry, larval filets were prepared in
554 Ringer solution and incubated with a rabbit anti-GFP antibody (1:50 in Ringer
555 solution, Life Technologies, Carlsbad, CA) for 1h on ice. Filets were washed with
556 Ringer solution (3x10 min at 4 °C) and then fixed with 4% Formaldehyde/PBS for
557 15min on ice. Subsequent steps including anti-mew and secondary antibody
558 incubation were carried out in the presence of 0.3% Triton X-100 as above.

559

560 *Quantitative Ret and integrin colocalization analysis*

561 3rd instar larval filet preparations immunostained for Ret and integrins were analyzed
562 by confocal microscopy with high resolution using a high NA oil objective (Zeiss
563 LSM700, 40x/NA1.3, z step size: 300nm). Confocal stacks covering the soma and
564 part of the dorsal field of ddaC neurons (xy dimension: 160x160 μm) were obtained
565 and deconvoluted using a blind deconvolution algorithm with an adaptive PSF
566 (AutoQuant, BitPlane AG, Zürich, Switzerland). Colocalization analysis was then
567 performed on the deconvolved confocal stacks in 3D using the Imaris Coloc module
568 (BitPlane AG, Zürich, Switzerland). The GFP reporter signal (*ppk-Gal4>UAS-CD8-*
569 *GFP or UAS-CD4-tdGFP*) was used to create a mask for the C4da neuron soma and
570 dendrite signal to specifically analyze neuronal integrin and Ret signals. Ret and
571 integrin signals were then automatically thresholded and colocalization was
572 calculated (Pearson coefficients, n=5 per genotype). Costes randomization was
573 performed for all samples to ensure that the calculated colocalization coefficients
574 between Ret and integrins are non-random (n=100 iterations, P=1 for all samples).

575

576 *Cell culture, immunocytochemistry and biochemistry*

577 S2 cells were grown at 25C in Schneider´s Drosophila Medium (Life Technologies,
578 Carlsbad, CA) with 10%FBS and Glutamine/Pen/Strep. For experiments, cells were
579 seeded in 6 well plates and transfected at 50% density in an adherent state using
580 Transfectene (Qiagen, Venlo, Netherlands). For S2 cell expression, UAS constructs
581 were co-transfected with pActin-Gal4. The following constructs were used: pUAST-
582 Ret-mCherry, pUAST-mys-3xflag-His, pUAST-mew.

583 For co-immunoprecipitation experiments, cells were harvested 48h after transfection
584 and lysed in 500ul lysis buffer (50mM Tris pH7.4, 150 mM NaCl, 1% Triton X-100) for
585 20 min on ice. After 10min/4C/10.000g centrifugation, supernatants were pre-
586 incubated with mouse IgG Agarose ((Sigma-Aldrich, St. Louis, MO) for 30min at 4 °C,
587 and then incubated with anti-flag M2 agarose beads (Sigma-Aldrich) for 4 h at 4 °C.
588 After extensive washing with lysis buffer, the samples were denatured and analyzed
589 on Tris-Acetate gels (Life Technologies, Carlsbad, CA) and Western Blotting against
590 Ret-mCherry (anti-DsRed, 1:1000, BD Clontech) and mys (anti-flag M2, 1:10.000,
591 Sigma).

592 For immunostaining, S2 cells were allowed to adhere to Concavalin A (Sigma-
593 Aldrich) coated cover slips for 1h and subsequently fixed in 4%
594 Paraformaldehyde/PBS solution for 10 min. After washing with PBS, cells were
595 permeabilized with 0.1% Triton X-100 for 10 min and blocked with 5% donkey
596 serum/PBS. Primary antibodies used were: rabbit anti-DsRed (1:500, BD Clontech,
597 Mountain Viev, CA), mouse anti-mew (1:100, DSHB), mouse anti-mys 1:100, DSHB).
598 Primary antibodies were applied over night at 4 °C in 5% donkey serum/PBS, while

secondary donkey antibodies with conjugated DyLight fluorophores (Jackson ImmunoResearch) were subsequently incubated for 1h at room temperature. Cells were mounted and imaged by confocal microscopy (Leica SP5 and Olympus FV1000).

In vivo confocal microscopy and time lapse imaging

C4da neurons of 3rd instar *Drosophila* larvae (72-100h AEL) were imaged alive by confocal microscopy (Leica SP5 or Olympus FV1000), using *ppk-CD4-tdTomato* or *ppk-Gal4, UAS-CD4-tdGFP* transgenes (Han et al., 2011). *Vkg-GFP* or *trol-GFP* trap lines labeling endogenous vkg or troll proteins with GFP were used to visualize the extracellular matrix. Confocal stacks were taken to image ddaC C4da neuron dendrite fields either with 20x (full ddaC field) or 40x oil objectives (dorsal ddaC field). For imaging dendrite-ECM interaction, two color high resolution confocal stacks using a high NA oil objective (Leica or Olympus, 40x, NA 1.3) were taken with a step size of 300 nm.

For time lapse imaging of C4da neurons in wildtype and *Ret* mutant animals*, ppk-Gal4, UAS-CD4-tdGFP* embryos were collected on grape agar plates for 2h and allowed to develop at 25 °C. Two C4da neurons per animal (abdominal segments a3 and a4) were imaged at 72h AEL, and the same neurons were imaged again 24h later (96h AEL). The imaged larvae were allowed to develop to adulthood to ensure that handling and imaging did not interfere with normal development.

Analysis of dendrite length, crossing, field coverage and ECM interaction

Dendrites of C4da neurons were traced with the Imaris Filament Tracer module (BitPlane AG, Zürich, Switzerland) using deconvoluted confocal stacks. Total dendritic length was calculated from the traces and Z-crossing points were counted and manually confirmed as non-contacting by visual inspection of the z-stack. The high resolution 3D reconstruction was done in Imaris. Dendritic field coverage was calculated essentially as described (Parrish et al., 2009) by measuring the area covered by dendrites (polygon formed by connecting all dendritic terminals of the field) divided by the total segment area using Fiji/ImageJ (NIH, Bethesda). Statistical significance was calculated by comparison of all genotypes using a Mann-Whitney test (Origin Pro, Origin Lab, Northhampton, MA).

To quantify net dendrite growth/retraction, confocal Z-projections of the same neuron at 72 and 96h AEL were overlayed and adjusted for position and interstitial growth with bUnwarpJ (Fiji, ImageJ). Landmarks marking all major branch points were used to get accurate overlay images. Growing (branch is shorter at 72h than 96h AEL) and retracting (branch is longer at 72h than 96h AEL) portions of dendrites were traced and growth/retraction values were normalized to the total length of the unchanged portion of the dendritic tree at 96h AEL. Statistical significance was calculated using a Student's two-tailed *t*-test.

Analysis of dendrite-ECM interaction was essentially performed as described (Han et al., 2012). Briefly, high resolution confocal stacks were deconvoluted using a blind deconvolution algorithm with an adaptive PSF (AutoQuant, BitPlane AG, Zürich, Switzerland). Dendrites were traced semi-automatically using the Imaris Filament Tracer module (Bitplane) and thresholded colocalization of the ECM and dendrite signals was performed. Non-contacting and contacting portions of the dendritic tree

were traced and verified manually. Percentages of detached dendrites were calculated by the ratios of detached vs. total dendrite length. Statistical significance was calculated by comparison of all genotypes using a Mann-Whitney test (Origin Pro).

Analysis of LifeAct expression and distribution

The dorsal field of C4da ddaC neurons expressing LifeAct-mCherry with *ppk-Gal4>CD-4tdGFP* was imaged with confocal microscopy at the 3rd instar larval stage (96-100h AEL). Acquired stacks were then processed with Fiji/ImageJ (NIH, Bethesda, MD) to normalize the LifeAct signal to GFP expression using a previously described procedure with minor adaptations (Kardash et al., 2011). Briefly, we used maximum projections of 2-color stacks and aligned the GFP and LifeAct channels using the TurboReg plugin (ImageJ). The LifeAct signal was threshholded automatically (ImageJ) and normalized to GFP levels using the RatioPlus plugin (ImageJ). For LifeAct quantification along major dendritic arbors, normalized intensity values were obtained by ROI tracing of 2 major branches per sample using the PlotProfile function (ImageJ, n=5 per genotype). Statistical significance was then calculated by using an Allometric fitting function ($y=a*x^b$, Origin Pro) for the intensity profiles of wildtype (average $R^2=0.74$) and Ret mutant (average $R^2=0.79$) samples and fit comparison of the two datasets ($p<0.05$, n=5 per genotype, Origin Pro).

Acknowledgements

We would like to thank: R. Cagan for the *Drosophila* Ret cDNA, J. Wildonger for generously sharing the *UAS-LifeAct-mCherry* transgene, and K. Duncan for S2 cells; J. Parrish, K. Duncan and F. Calderon de Anda for comments on the manuscript, the

671 Bloomington, Kyoto and VDRC stock centers for transgenic fly lines; the
672 Developmental Studies Hybridoma Bank (DSHB) and its contributors for the integrin
673 antibodies. L. Y. J. and Y. N. J. are investigators of the Howard Hughes Medical
674 Institute.

675

676 **Competing Interests**

677 The authors declare that no competing interests exist.

678

References

Abrescia, C., Sjöstrand, D., Kjaer, S., and Ibáñez, C.F. (2005). Drosophila RET contains an active tyrosine kinase and elicits neurotrophic activities in mammalian cells. FEBS Lett. *579*, 3789–3796.

Airaksinen, M.S., Holm, L., and Hätinen, T. (2006). Evolution of the GDNF family ligands and receptors. Brain. Behav. Evol. *68*, 181–190.

Almeida, M.Q., and Hoff, A.O. (2012). Recent advances in the molecular pathogenesis and targeted therapies of medullary thyroid carcinoma. Curr. Opin. Oncol. *24*, 229–234.

Amiel, J., Sproat-Emison, E., Garcia-Barcelo, M., Lantieri, F., Burzynski, G., Borrego, S., Pelet, A., Arnold, S., Miao, X., Griseri, P., et al. (2008). Hirschsprung disease, associated syndromes and genetics: a review. J. Med. Genet. *45*, 1–14.

Bonanomi, D., Chivatakarn, O., Bai, G., Abdesselem, H., Lettieri, K., Marquardt, T., Pierchala, B. a, and Pfaff, S.L. (2012). Ret is a multifunctional coreceptor that integrates diffusible- and contact-axon guidance signals. Cell *148*, 568–582.

Bourane, S., Garces, A., Venteo, S., Pattyn, A., Hubert, T., Fichard, A., Puech, S., Boukhaddaoui, H., Baudet, C., Takahashi, S., et al. (2009). Low-threshold mechanoreceptor subtypes selectively express MafA and are specified by Ret signaling. Neuron *64*, 857–870.

Chen, T.T., Luque, A., Lee, S., Anderson, S.M., Segura, T., and Iruela-Arispe, M.L. (2010). Anchorage of VEGF to the extracellular matrix conveys differential signaling responses to endothelial cells. J. Cell Biol. *188*, 595–609.

Cockburn, J.G., Richardson, D.S., Gujral, T.S., and Mulligan, L.M. (2010). RET-mediated cell adhesion and migration require multiple integrin subunits. J. Clin. Endocrinol. Metab. *95*, E342–E346.

Dar, A.C., Das, T.K., Shokat, K.M., and Cagan, R.L. (2012). Chemical genetic discovery of targets and anti-targets for cancer polypharmacology. Nature *486*, 80–84.

Dietzl, G., Chen, D., Schnorrer, F., Su, K.C., Barinova, Y., Fellner, M., Gasser, B., Kinsey, K., Oppel, S., Scheiblauer, S., et al. (2007). A genome-wide transgenic RNAi library for conditional gene inactivation in Drosophila. Nature *448*, 151–156.

Dimitrova, S., Reissaus, A., and Tavosanis, G. (2008). Slit and Robo regulate dendrite branching and elongation of space-filling neurons in Drosophila. Dev. Biol. *324*, 18–30.

Dong, X., Liu, O.W., Howell, A.S., and Shen, K. (2013). An Extracellular Adhesion Molecule Complex Patterns Dendritic Branching and Morphogenesis. Cell *155*, 296–307.

716 Dudanova, I., and Klein, R. (2013). Integration of guidance cues: parallel signaling
717 and crosstalk. Trends Neurosci. *36*, 295–304.

718 Egea, J., and Klein, R. (2007). Bidirectional Eph-ephrin signaling during axon
719 guidance. Trends Cell Biol. *17*, 230–238.

720 Emoto, K., He, Y., Ye, B., Grueber, W.B., Adler, P.N., Jan, L.Y., and Jan, Y.N.
721 (2004). Control of dendritic branching and tiling by the Tricornered-kinase/Furry
722 signaling pathway in Drosophila sensory neurons. Cell *119*, 245–256.

723 Emoto, K., Parrish, J.Z., Jan, L.Y., and Jan, Y.N. (2006). The tumour suppressor
724 Hippo acts with the NDR kinases in dendritic tiling and maintenance. Nature *443*,
725 210–213.

726 Fuerst, P.G., Koizumi, A., Masland, R.H., and Burgess, R.W. (2008). Neurite
727 arborization and mosaic spacing in the mouse retina require DSCAM. Nature *451*,
728 470–474.

729 Fuerst, P.G., Bruce, F., Tian, M., Wei, W., Elstrott, J., Feller, M.B., Erskine, L.,
730 Singer, J.H., and Burgess, R.W. (2009). DSCAM and DSCAML1 function in self-
731 avoidance in multiple cell types in the developing mouse retina. Neuron *64*, 484–497.

732 Fukuda, T., Kiuchi, K., and Takahashi, M. (2002). Novel mechanism of regulation of
733 Rac activity and lamellipodia formation by RET tyrosine kinase. J. Biol. Chem. *277*,
734 19114–19121.

735 Gibson, D. a, Tymanskyj, S., Yuan, R.C., Leung, H.C., Lefebvre, J.L., Sanes, J.R.,
736 Chédotal, A., and Ma, L. (2014). Dendrite self-avoidance requires cell-autonomous
737 slit/robo signaling in cerebellar purkinje cells. Neuron *81*, 1040–1056.

738 Groth, A.C., Fish, M., Nusse, R., and Calos, M.P. (2004). Construction of transgenic
739 Drosophila by using the site-specific integrase from phage phiC31. Genetics *166*,
740 1775–1782.

741 Grueber, W.B., and Sagasti, A. (2010). Self-avoidance and tiling: Mechanisms of
742 dendrite and axon spacing. Cold Spring Harb Perspect Biol *2*, a001750.

743 Grueber, W.B., Jan, L.Y., and Jan, Y.N. (2002). Tiling of the Drosophila epidermis by
744 multidendritic sensory neurons. Development *129*, 2867–2878.

745 Hahn, M., and Bishop, J. (2001). Expression pattern of Drosophila ret suggests a
746 common ancestral origin between the metamorphosis precursors in insect endoderm
747 and the vertebrate enteric neurons. Proc. Natl. Acad. Sci. U. S. A. *98*, 1053–1058.

748 Hakeda-Suzuki, S., Ng, J., Tzu, J., Dietzl, G., Sun, Y., Harms, M., Nardine, T., Luo,
749 L., and Dickson, B.J. (2002). Rac function and regulation during Drosophila
750 development. Nature *416*, 438–442.

751 Han, C., Jan, L.Y., and Jan, Y.-N.N. (2011). Enhancer-driven membrane markers for
752 analysis of nonautonomous mechanisms reveal neuron-glia interactions in
753 Drosophila. Proc Natl Acad Sci U S A *108*, 9673–9678.

754 Han, C., Wang, D., Soba, P., Zhu, S., Lin, X., Jan, L.Y., and Jan, Y.-N. (2012).
755 Integrins regulate repulsion-mediated dendritic patterning of drosophila sensory
756 neurons by restricting dendrites in a 2D space. Neuron *73*, 64–78.

757 Hattori, D., Chen, Y., Matthews, B.J., Salwinski, L., Sabatti, C., Grueber, W.B., and
758 Zipursky, S.L. (2009). Robust discrimination between self and non-self neurites
759 requires thousands of Dscam1 isoforms. Nature *461*, 644–648.

760 Hughes, M.E., Bortnick, R., Tsubouchi, A., Bäumer, P., Kondo, M., Uemura, T., and
761 Schmucker, D. (2007). Homophilic Dscam interactions control complex dendrite
762 morphogenesis. Neuron *54*, 417–427.

763 Ivaska, J., and Heino, J. (2011). Cooperation between integrins and growth factor
764 receptors in signaling and endocytosis. Annu. Rev. Cell Dev. Biol. *27*, 291–320.

765 Jan, Y.N., and Jan, L.Y. (2010). Branching out: mechanisms of dendritic arborization.
766 Nat Rev Neurosci *11*, 316–328.

767 Kallijärvi, J., Stratoulias, V., Virtanen, K., Hietakangas, V., Heino, T.I., and Saarma,
768 M. (2012). Characterization of Drosophila GDNF receptor-like and evidence for its
769 evolutionarily conserved interaction with neural cell adhesion molecule (NCAM)/FasII.
770 PLoS One *7*, e51997.

771 Kardash, E., Bandemer, J., and Raz, E. (2011). Imaging protein activity in live
772 embryos using fluorescence resonance energy transfer biosensors. Nat. Protoc. *6*,
773 1835–1846.

774 Kim, M.E., Shrestha, B.R., Blazeski, R., Mason, C. a, and Grueber, W.B. (2012).
775 Integrins establish dendrite-substrate relationships that promote dendritic self-
776 avoidance and patterning in drosophila sensory neurons. Neuron *73*, 79–91.

777 Koike-Kumagai, M., Yasunaga, K., Morikawa, R., Kanamori, T., and Emoto, K.
778 (2009). The target of rapamycin complex 2 controls dendritic tiling of Drosophila
779 sensory neurons through the Tricornered kinase signalling pathway. EMBO J. *28*,
780 3879–3892.

781 Kowsky, S., Pöppelmeyer, C., Kramer, E.R., Falkenburger, B.H., Kruse, A., Klein, R.,
782 and Schulz, J.B. (2007). RET signaling does not modulate MPTP toxicity but is
783 required for regeneration of dopaminergic axon terminals. Proc. Natl. Acad. Sci. U. S.
784 A. *104*, 20049–20054.

785 Kramer, E.R., Knott, L., Su, F., Dessaud, E., Krull, C.E., Helmbacher, F., and Klein,
786 R. (2006). Cooperation between GDNF/Ret and ephrinA/EphA4 signals for motor-
787 axon pathway selection in the limb. Neuron *50*, 35–47.

788 Kramer, E.R., Aron, L., Ramakers, G.M.J., Seitz, S., Zhuang, X., Beyer, K., Smidt,
789 M.P., and Klein, R. (2007). Absence of Ret signaling in mice causes progressive and
790 late degeneration of the nigrostriatal system. PLoS Biol. *5*, e39.

Kuhn, T.B., Brown, M.D., and Bamburg, J.R. (1998). Rac1-dependent actin filament organization in growth cones is necessary for beta1-integrin-mediated advance but not for growth on poly-D-lysine. J. Neurobiol. *37*, 524–540.

Lairmore, T.C., Dou, S., Howe, J.R., Chi, D., Carlson, K., Veile, R., Mishra, S.K., Wells, S.A., and Donis-Keller, H. (1993). A 1.5-megabase yeast artificial chromosome contig from human chromosome 10q11.2 connecting three genetic loci (RET, D10S94, and D10S102) closely linked to the MEN2A locus. Proc. Natl. Acad. Sci. U. S. A. *90*, 492–496.

Lee, T., and Luo, L. (1999). Mosaic analysis with a repressible cell marker for studies of gene function in neuronal morphogenesis. Neuron *22*, 451–461.

Lee, A., Li, W., Xu, K., Bogert, B. a, Su, K., and Gao, F.-B. (2003). Control of dendritic development by the Drosophila fragile X-related gene involves the small GTPase Rac1. Development *130*, 5543–5552.

Lefebvre, J.L., Kostadinov, D., Chen, W. V, Maniatis, T., and Sanes, J.R. (2012). Protocadherins mediate dendritic self-avoidance in the mammalian nervous system. Nature *488*, 517–521.

Long, H., Ou, Y., Rao, Y., and van Meyel, D.J. (2009). Dendrite branching and self-avoidance are controlled by Turtle, a conserved IgSF protein in Drosophila. Development *136*, 3475–3484.

Luo, W., Enomoto, H., Rice, F.L., Milbrandt, J., and Ginty, D.D. (2009). Molecular identification of rapidly adapting mechanoreceptors and their developmental dependence on ret signaling. Neuron *64*, 841–856.

Matsubara, D., Horiuchi, S.-Y., Shimono, K., Usui, T., and Uemura, T. (2011). The seven-pass transmembrane cadherin Flamingo controls dendritic self-avoidance via its binding to a LIM domain protein, Espinas, in Drosophila sensory neurons. Genes Dev. *25*, 1982–1996.

Matthews, B.J., and Grueber, W.B. (2011). Dscam1-mediated self-avoidance counters netrin-dependent targeting of dendrites in Drosophila. Curr. Biol. *21*, 1480–1487.

Matthews, B.J., Kim, M.E., Flanagan, J.J., Hattori, D., Clemens, J.C., Zipursky, S.L., and Grueber, W.B. (2007). Dendrite self-avoidance is controlled by Dscam. Cell *129*, 593–604.

Ng, J., Nardine, T., Harms, M., Tzu, J., Goldstein, A., Sun, Y., Dietzl, G., Dickson, B.J., and Luo, L. (2002). Rac GTPases control axon growth, guidance and branching. Nature *416*, 442–447.

Pachnis, V., Mankoo, B., and Costantini, F. (1993). Expression of the c-ret proto-oncogene during mouse embryogenesis. Development *119*, 1005–1017.

828 Parrish, J.Z., Emoto, K., Jan, L.Y., and Jan, Y.N. (2007). Polycomb genes interact
829 with the tumor suppressor genes hippo and warts in the maintenance of Drosophila
830 sensory neuron dendrites. Genes Dev *21*, 956–972.

831 Parrish, J.Z., Xu, P., Kim, C.C., Jan, L.Y., and Jan, Y.N. (2009). The microRNA
832 bantam functions in epithelial cells to regulate scaling growth of dendrite arbors in
833 drosophila sensory neurons. Neuron *63*, 788–802.

834 Read, R.D., Goodfellow, P.J., Mardis, E.R., Novak, N., Armstrong, J.R., and Cagan,
835 R.L. (2005). A Drosophila model of multiple endocrine neoplasia type 2. Genetics
836 *171*, 1057–1081.

837 Riedl, J., Crevenna, A.H., Kessenbrock, K., Yu, J.H., Neukirchen, D., Bista, M.,
838 Bradke, F., Jenne, D., Holak, T.A., Werb, Z., et al. (2008). Lifeact: a versatile marker
839 to visualize F-actin. Nat. Methods *5*, 605–607.

840 Runeberg-Roos, P., and Saarma, M. (2007). Neurotrophic factor receptor RET:
841 structure, cell biology, and inherited diseases. Ann. Med. *39*, 572–580.

842 Salzberg, Y., Díaz-Balzac, C.A., Ramirez-Suarez, N.J., Attreed, M., Tecle, E.,
843 Desbois, M., Kaprielian, Z., and Bülow, H.E. (2013). Skin-Derived Cues Control
844 Arborization of Sensory Dendrites in Caenorhabditis elegans. Cell *155*, 308–320.

845 Schuchardt, A., D'Agati, V., Larsson-Blomberg, L., Costantini, F., and Pachnis, V.
846 (1994). Defects in the kidney and enteric nervous system of mice lacking the tyrosine
847 kinase receptor Ret. Nature *367*, 380–383.

848 Soba, P., Zhu, S., Emoto, K., Younger, S., Yang, S.-J.J., Yu, H.-H.H., Lee, T., Jan,
849 L.Y., and Jan, Y.-N.N. (2007). Drosophila sensory neurons require Dscam for
850 dendritic self-avoidance and proper dendritic field organization. Neuron *54*, 403–416.

851 Spitzweck, B., Brankatschk, M., and Dickson, B.J. (2010). Distinct protein domains
852 and expression patterns confer divergent axon guidance functions for Drosophila
853 Robo receptors. Cell *140*, 409–420.

854 Sugaya, R., Ishimaru, S., Hosoya, T., Saigo, K., and Emori, Y. (1994). A Drosophila
855 homolog of human proto-oncogene ret transiently expressed in embryonic neuronal
856 precursor cells including neuroblasts and CNS cells. Mech. Dev. *45*, 139–145.

857 Yamamoto, M., Ueda, R., Takahashi, K., Saigo, K., and Uemura, T. (2006). Control
858 of axonal sprouting and dendrite branching by the Nrg-Ank complex at the neuron-
859 glia interface. Curr Biol *16*, 1678–1683.

860 Zipursky, S.L., and Sanes, J.R. (2010). Chemoaffinity revisited: dscams,
861 protocadherins, and neural circuit assembly. Cell *143*, 343–353.

862

863

Figure Legends

Figure 1: *In vivo* RNAi knockdown of *Ret* causes C4da neuron dendrite pattering defects.

(A) Ret^{RNAi} transgenes together with *Dcr2* were driven by $Gal4^{21\text{-}7}$ and C4da neuron morphology was visualized with a specific fluorescent reporter (*ppk-CD4-tdTomato*). Confocal live images of control animals (ctl) show wildtype dendrite morphology, while expression of either of two independent *Ret-RNAi* transgenes led to severely disorganized dendrites with incomplete receptive field coverage. (B) A Gal4 insertion in the *Ret* genomic locus drives CD8-GFP expression in C4da neurons indicating the presence of Ret. Scale bar 50 μm. (C-E) Immunohistochemical analysis of Ret expression in 3rd instar larvae of wildtype (C,D) and *Ret* deficient animals (E). Overlays with GFP expressing C4da neurons (*ppk-Gal4>CD4-tdGFP*) show that specific anti-Ret signal could be detected throughout the C4da dendritic arbor (C). Resliced portions (in Z direction) of primary (C') and terminal (C'') C4da dendrites show that Ret strongly labels the basal side of dendrites facing the ECM as shown in the schematic drawing. (D) Ret was also present in distal terminal dendrites of the dorsal field of C4da neurons (D',D'', scale bar 20 μm, 10 μm for insets). Residual Ret signal was detected in the C4da neuron soma in *Ret* mutant animals but not in dendrites (E inset). Arrows indicate non-specific antibody signal present in wildtype and *Ret* mutant samples. Scale bar 20 μm. (F) Quantitative analysis of Ret immunoreactivity in C4da somata of wildtype and *Ret* mutant samples showing the signal over background ($\Delta F/F$, mean ±SD, n=5, $p<0.001$, Student's two-tailed *t*-test).

Figure 2: Loss of *Ret* function impairs C4da neuron dendrite patterning and results in out of plane crossing of isoneuronal branches.

(A-C) Confocal live images of C4da neurons in (A) wildtype, (B) Ret^{C168} homozygous and (C) $Ret^{C168}/Df(Bsc^{312})$ 3rd instar larvae. Loss of Ret function causes abnormal dendrite patterning featuring reduced receptive field coverage and overlapping dendrites (indicated by arrows). Note that the phenotype is more severe in $Ret^{C168}/Df(Bsc^{312})$ than in Ret^{C168} mutant C4da neurons. Scale bar: 50 μm. (D) 3D reconstruction of a *Ret* deficient C4da neuron with magnified 3D views of regions with dendrites crossing in different growth planes (D',D''). Scale bar: 25 μm. (E) Total dendrite length of *Ret* mutant C4da neurons was not significantly changed compared to wildtype. Out of plane crossing of C4da neuron dendrites in *Ret* mutants was however highly elevated (mean ±SD, n=8; $p<0.001$, Student's two-tailed *t*-test).

Figure 3: Dendrite-ECM detachment due to *Ret* loss of function is genetically linked to integrins.

C4da neuron dendrites along the dorsal midline (*ppk-CD4-tdTomato*) and the extracellular matrix (*trol-GFP* or *vkg-GFP*) were co-visualized in 3rd instar larvae. High resolution two-color confocal z-stacks were analyzed for dendrite-ECM interaction and detached dendrite segments are indicated in magenta as indicated schematically. (A) In wildtype animals, very few dendrite segments were not in contact with the ECM. Magnified regions of (A) and cross sections illustrate dendrite-ECM proximity with few dendrite segments not contacting the ECM (A', A'', ECM in green, dendrites in magenta, see schematic for color code). (B) A strong increase of detached dendrites could be observed in *Ret* mutant animals, highlighted in the magnified sections displaying severe displacement of dendrites from the ECM (B',

B''). Scale bar: 25 μm. (C) Quantitative analysis of dendrite-ECM interaction in *wildtype* and *Ret* mutant C4da neurons revealed a strong increase in dendrite detachment in *Ret* deficient animals (mean ±SD, n=5, p<0.001, Student's two-tailed *t*-test). (D-E) Genetic interaction analysis of dendrite-ECM adhesion in (D) Ret^{C168}, (E) mew^{M6}, (F) mys^{1} heterozygous and (G) mew^{M6}/Ret^{C168} (H) mys^{1}/Ret^{C168} trans-heterozygous 3rd instar larvae. The combination of either integrin mutant with the Ret^{C168} allele showed highly increased loss of dendrite-ECM interaction (G,H) compared to wildtype or the heterozygous alleles alone. Scale bar: 25 μm. (I) Quantitative analysis of dendrite detachment for the individual genotypes as indicated. mew^{M6}/Ret^{C168} and mys^{1}/Ret^{C168} trans-heterozygotes showed significantly impaired dendrite-ECM adhesion (mean ±SD, p<0.05, n=4, Mann-Whitney U-test).

Figure 4: Ret localizes to the dendrite surface and co-localizes with integrins.

(A) Cell surface immunostaining of pHluorin-Ret-mCherry expressed in C4da neurons using *ppk-Gal4*. Surface exposed Ret labeled by pHluorin (surface-stained with anti-GFP antibody) showed even labeling of the entire dendritic tree, while the mCherry signal displayed a more granular distribution of cellular Ret. Scale bar: 30 μm. (B) Cell surface immunostaining of pHluorin-Ret-mCherry co-expressing mys and mew in C4da neurons using *ppk-Gal4.* Cell surface and cellular Ret were partially co-distributed with Mew in dendrites, as evident from fluorescence intensity plots along (B') low order and (B'') terminal dendrites. Scale bar 20 μm. (C) Quantitative colocalization analysis of Ret and integrins coexpressed in C4da neurons (*ppk-Gal4,CD8-GFP>Ret-mCherry,mys,mew*). Pearson coefficients were calculated for C4da neuron soma and dendrite regions showing a positive correlation of Ret and integrin signals (see Methods for details, mean ±SD, n=5 per genotype).

(D,E) Colocalization analysis of endogenous Ret and integrins overexpressed in C4da neurons (*ppk-Gal4,CD4-tdGFP> mys,mew*). Endogenous Ret signal was colocalized with (D) anti-mys or (E) anti-mew immunoreactivity in C4da neurons and colocalized pixels visualized in false color representations (coloc). (D',E') Stretches of terminal dendrites resliced in Z direction showing partial colocalization of (D') Ret and mys or (E') Ret and mew along the basal dendrite facing the ECM as indicated by arrows (see schematic drawing). Line intensity plots of the same dendrite portion show signal distribution of endogenous Ret and integrins together with the colocalized signals (coloc) and the CD4-tdGFP membrane marker. (D'',E'') Line intensity plots for a primary dendrite portion (indicated in D and E). (F) Quantitative colocalization analysis of endogenous Ret and integrins expressed in C4da neurons (*ppk-Gal4,CD4-tdGFP>mys,mew*). Pearson coefficients calculated for C4da neuron soma and dendrites showing a positive correlation of endogenous Ret and integrin signals (see Methods for details, mean ±SD, n=5 per genotype).

Figure 5: Cell-autonomous rescue of *Ret* mutant dendrite defects by class IV-specific expression of Ret or integrins.

(A-D) Maximum projections of C4da neurons visualized with *ppk-Gal4>CD4-tdGFP* are shown for (A) wildtype and (B-D) *Ret* mutant animals. C4da neuron specific expression of (C) *UAS-Ret-mCherry* or (D) *UAS-mys/UAS-mew* in *Ret* mutant larvae rescues dendrite crossing defects. However, only re-expression of Ret fully restores dendritic field coverage to wildtype levels. Scale bar 100 μm. (A'-D') Magnified view of the indicated dendrite area for the different genotypes. Dendrite crossing points are indicated by arrowheads. Note that Ret-mCherry or integrin expression in Ret mutant C4da neurons strongly reduced dendrite crossing events. Scale bar 30 μm.

(E) Quantitative analysis of out of plane dendrite crossing for the indicated genotypes. Re-expression of Ret or integrins specifically in C4da neurons of *Ret* mutant animals fully rescues dendrite crossing defects ($p<0.001$, n=5) (F) Dendrite coverage index (ratio of dendrite field area and segment area (Parrish et al., 2009) is shown for the indicated genotypes. Defects in receptive field coverage of *Ret* mutant C4da neurons are rescued by C4da specific expression of the Ret-mCherry transgene, but not integrin overexpression (mean ±SD, $p<0.001$, n=5, Mann-Whitney U-test).

Figure 6: Rac1 loss of function phenocopies and genetically interacts with Ret and integrins.

The dorsal field of C4da neurons (*ppk-CD4-Tom*) and the extracellular matrix (*vkg-GFP*) were co-visualized in 3rd instar larvae. High resolution two-color confocal z-stacks were analyzed for dendrite-ECM interaction and enclosed dendrite segments are indicated in magenta. Images of (A) Wildtype (B) $rac1^{J11}$ homozygous and (C) $rac1^{J11}$/ $rac1^{J10}$,$rac2^{\Delta}$,mtl^{Δ} larvae are shown displaying a strong increase of detached dendrites in the *rac1* mutant animals. Scale bar 30 μm. (D, E) Quantitative analysis of dendrite-ECM interaction and dendrite crossing in *wildtype* and *rac1* mutants shows a significant increase in dendrite detachment (C) and Z crossing points (D) in *rac1* deficient C4da neurons. (F-L) Genetic interaction analysis of dendrite-ECM adhesion in (F) *Ret*, (G) *mew*, (H) *mys* (I) *rac1* heterozygous and (J) *rac1*/*Ret* (K) *mew*/*rac1* (L) *mys*/*rac1* trans-heterozygous 3rd instar larvae. The combination of rac1 mutants with either *Ret* or integrins showed increased loss of dendrite-ECM interaction illustrated by detached portions of the dendritic tree (in magenta) Scale bar 30 μm. (M) Quantitative analysis of dendrite detachment from the ECM for the individual

genotypes as indicated (mean ±SD, $p<0.05$, n=4 per genotype, Mann-Whitney U-test).

Figure 7: Ret mutant C4da neurons display increased dendrite dynamics and aberrant F-actin localization.

(A-B) The dorsal dendrite field of the same C4da neurons expressing CD4-tdGFP was imaged at 72h and 96h AEL in (A) wildtype and (B) *Ret* mutant animals. Growth and retraction events of dendritic branches were traced and are highlighted in green (growing dendrite) and magenta (retracting dendrite). Scale bar 25 μm. (C) Quantitative analysis of dendrite growth and retraction events in wildtype and *Ret* mutant C4da neurons showing the relative change in dendrite length normalized by the total dendrite length of the dorsal field. Note that growth and retraction of dendrites in Ret mutant neurons is strongly increased (mean ±SD, $p<0.01$ for growth, $p<0.05$ for retraction, n=4,). (D) Dendrite growth/retraction ratios of *Ret* deficient C4da neurons show a significant decrease compared to wildtype (mean ±SD, $p<0.05$, n=4, Student's *t*-test). (E) F-actin levels in primary branches of *Ret* mutant C4da neurons are elevated in proximal regions compared to wildtype. Normalized LifeAct-mCherry signal along primary dendrites was plotted against increasing soma distance showing significantly different intensity profiles (shaded area ±SD, $p<0.05$, n=5). (F-G) Dorsal fields of ddaC neurons expressing CD4-tdGFP and LifeAct-mCherry were imaged at 96-100h AEL in (F) wildtype and (G) *Ret* mutant animals. LifeAct levels normalized to GFP are shown as color coded arbitrary intensities. *Ret* mutant C4da neuron dendrites display increased proximal, but reduced distal F-actin levels. Abnormal accumulation of F-actin in aberrant, crossing dendrites was frequently seen in *Ret* mutant but not wildtype neurons (indicated by arrows).

1012 Additionally, many terminal branches of *Ret* loss of function neurons have lower
1013 levels (below threshold) of F-actin than wildtype. Scale bar 30 μm.

1014

1015

Figure supplements

Figure 1-figure supplement 1: Class I da neurons do not display obvious morphological defects in Ret mutant animals

Ret^{C168} homozygous 3rd instar larvae display no obvious phenotype in class I da neuron morphology visualized by *2-21-Gal4>CD8-GFP*. Scale bar 50 μm.

Figure 1-figure supplement 2: *phospho-Ret* levels are reduced in Ret mutant C4da neurons.

(A,B) Immunohistochemical analysis of phospho-Ret in 3rd instar larvae of wildtype (A) and *Ret* mutant animals (B). Specific anti-phospho-Ret signal could be detected in C4da neuron somata of control but not *Ret* mutant animals (A,B inset). Arrows indicate non-specific antibody signal at epithelial junctions. Scale bar 25μm. Quantitative analysis of phospho-Ret immunoreactivity in C4da somata of wildtype and *Ret* mutant samples showing signal over background (ΔF/F, mean ±SD, n=3, $p<0.05$, Student's two-tailed *t*-test).

Figure 4-figure supplement 1: Colocalization and biochemical interaction of Ret and integrins in S2 cells

(A) Analysis in 3rd instar larval fillet preparations expressing Ret-mCherry (anti-DsRed immunostaining) in class IV da neurons with ppk-Gal4>CD8-GFP (anti-GFP). Ret was fairly evenly distributed in low and high order dendrites and the axon (yellow arrow). Scale bar 25 μm. (B) S2 cells were co-transfected with mys and Ret and imunostained with specific anti-mys (green) and anti-Ret antibodies (magenta). Mys and Ret co-localization in S2 cells is particularly strong in filopodial tips (arrows).

Scale bar 1 μm. (C) S2 cells were transfected with V5-tagged Ret and flag-tagged mys with or without mew co-transfection. Mys-flag was immunoprecipitated and Ret interaction was probed by Western blotting with an anti-V5 antibody. The asterisks indicate secondary antibody cross-reactivity with the IP antibody.

Figure 4-figure supplement 2: Overexpressed Ret and mys colocalization in C4da neurons.

(A) Immunohistochemical analysis of C4da neurons co-expressing Ret-mCherry with Mys/Mew using *ppk-Gal4>CD8-GFP*. Ret-mCherry signal was colocalized with anti-Mys immunoreactivity in C4da neurons and colocalized pixels visualized in false color representations (coloc). Ret and Mys showed co-localized punctae in dendritic arbors (indicated by arrows). Scale bar 20 μm. (A') High magnification view and cross-sections (indicated by yellow rectangle, Z cutting plane indicated by dashed lines) shows 3D co-localization of Ret and Mys in dendrites. (A'') Line intensity plot along a dendrite portion (indicated by dashed yellow line in A') show the signal covariance of Ret and Mys.

Figure 4-figure supplement 3: Overexpressed Ret and mew colocalization in C4da neurons.

(A,B) Immunohistochemical analysis of C4da neurons co-expressing Ret-mCherry with integrins Mys/Mew using *ppk-Gal4>CD8-GFP*. Ret and Mew colocalized pixels were visualized in false color representations (coloc) and co-localized punctae are present in dendritic arbors (indicated by arrows). Scale bar 20 μm. (A') High magnification view and cross-sections (indicated by yellow rectangle, Z cutting plane indicated by dashed lines) shows 3D co-localization of Ret and Mew in dendrites.

(A'') Line plots of signal intensities along a dendrite portion (indicated by dashed yellow line in A') show covariance of Ret and Mew localization.

Video 1: Colocalization of endogenous Ret and the integrin Mew in C4da neurons

The movie shows a 3-dimensional flight view of Ret-Mew colocalization along the C4da dendritic arbor. Shown are CD4-tdGFP labeling the C4da neuron (green), anti-Ret (magenta) and anti-Mew (cyan) together with the colocalized signal (grayscale) between Ret and Mew.

Figure 5-figure supplement 1: Integrins supress Ret overexpression induced adult eye phenotypes

Integrin co-expression suppresses Ret induced photoreceptor degeneration. Overexpression of Ret with *GMR-Gal4* caused a rough eye phenotype and pigmentation defects, which can be fully rescued by coexpression of integrins. Co-expression of Ret-mCherry and Mys-GFP could be readily detected by their fluorescent tag confirming the presence of both proteins in the rescued eye. Note that although Ret dependent photoreceptor phenotype was rescued, pigmentation defects observed upon Ret overexpression were not.

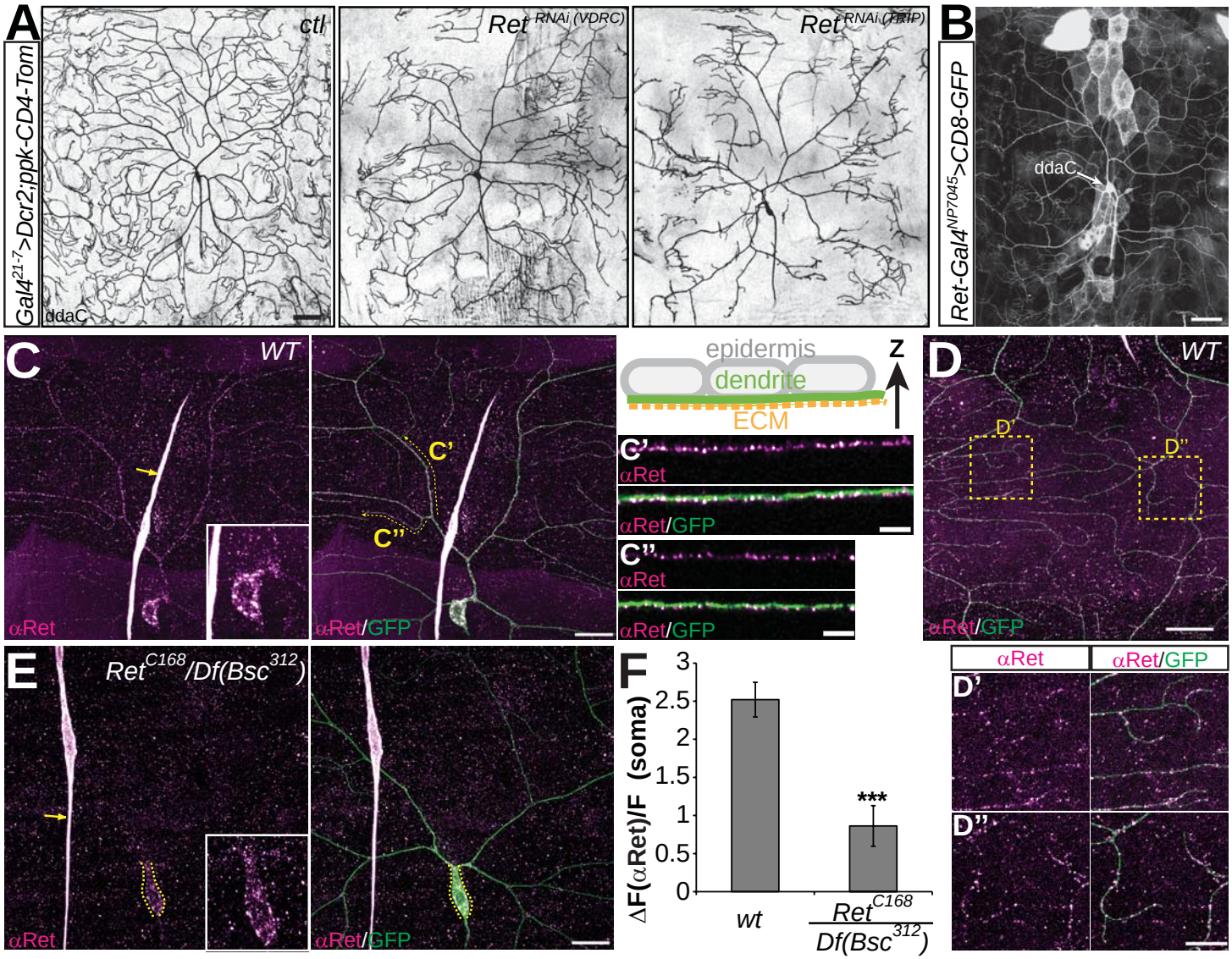


Figure 1, Soba *et al.*

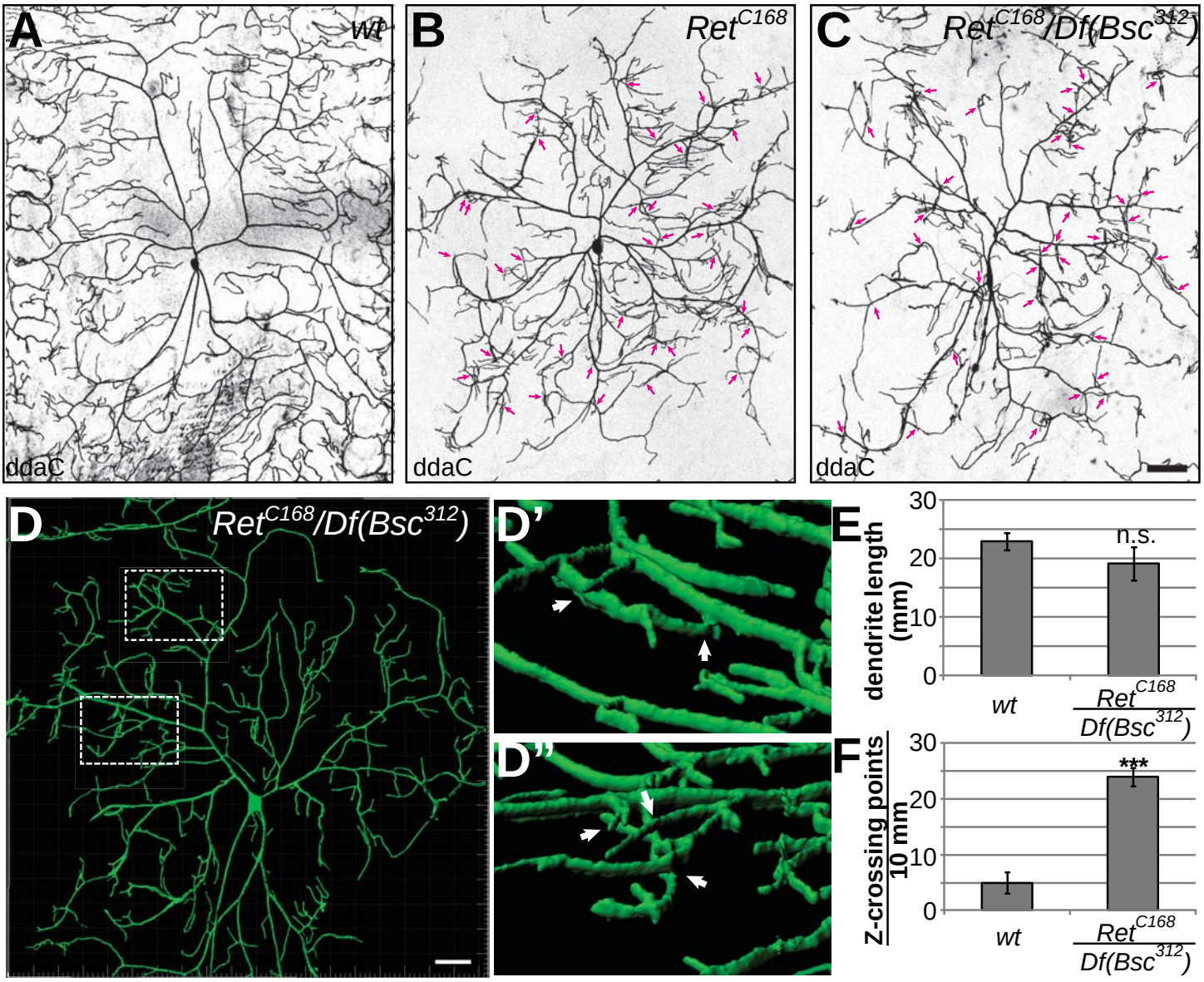


Figure 2, Soba *et al.*

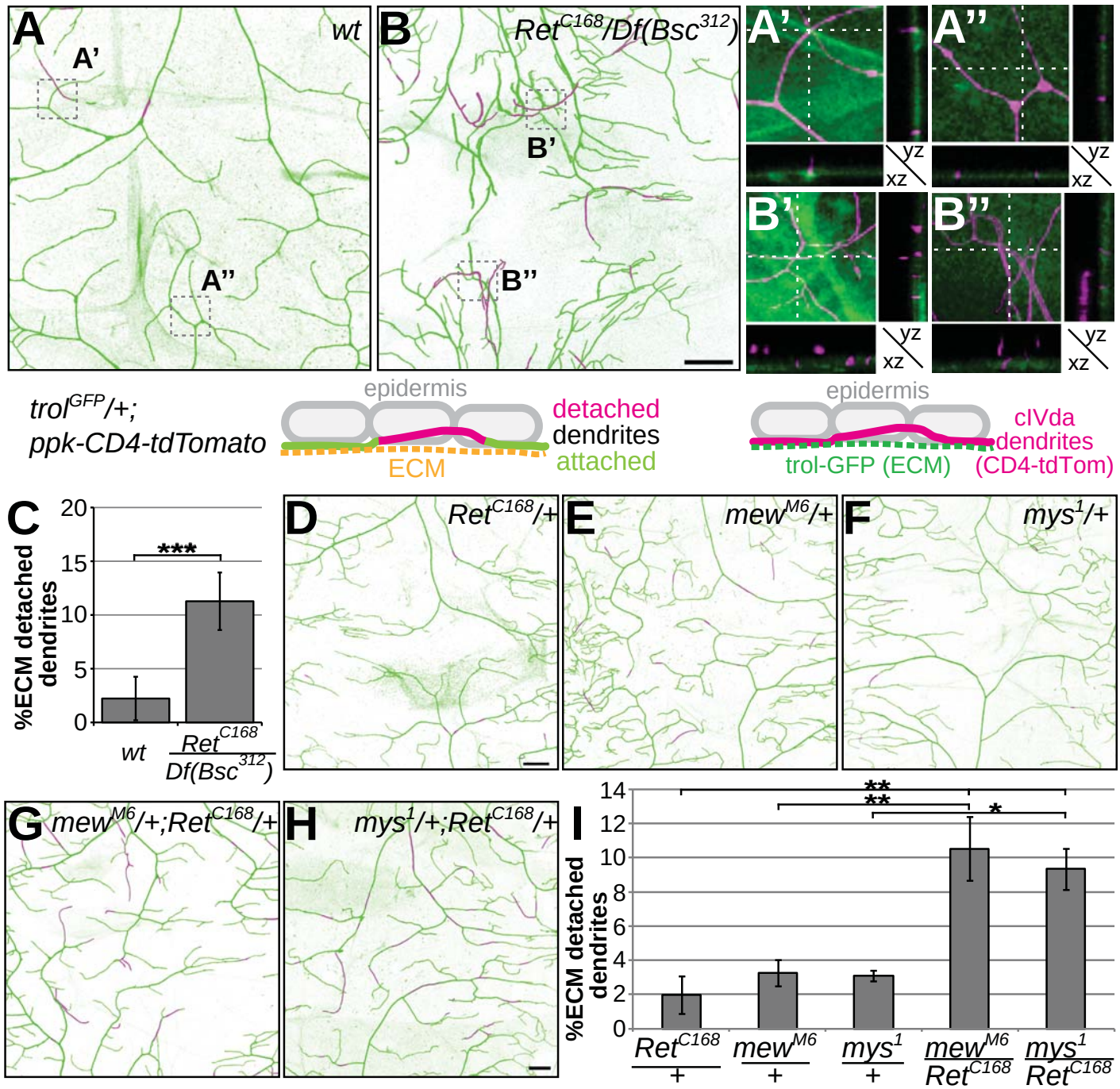


Figure 3, Soba *et al.*

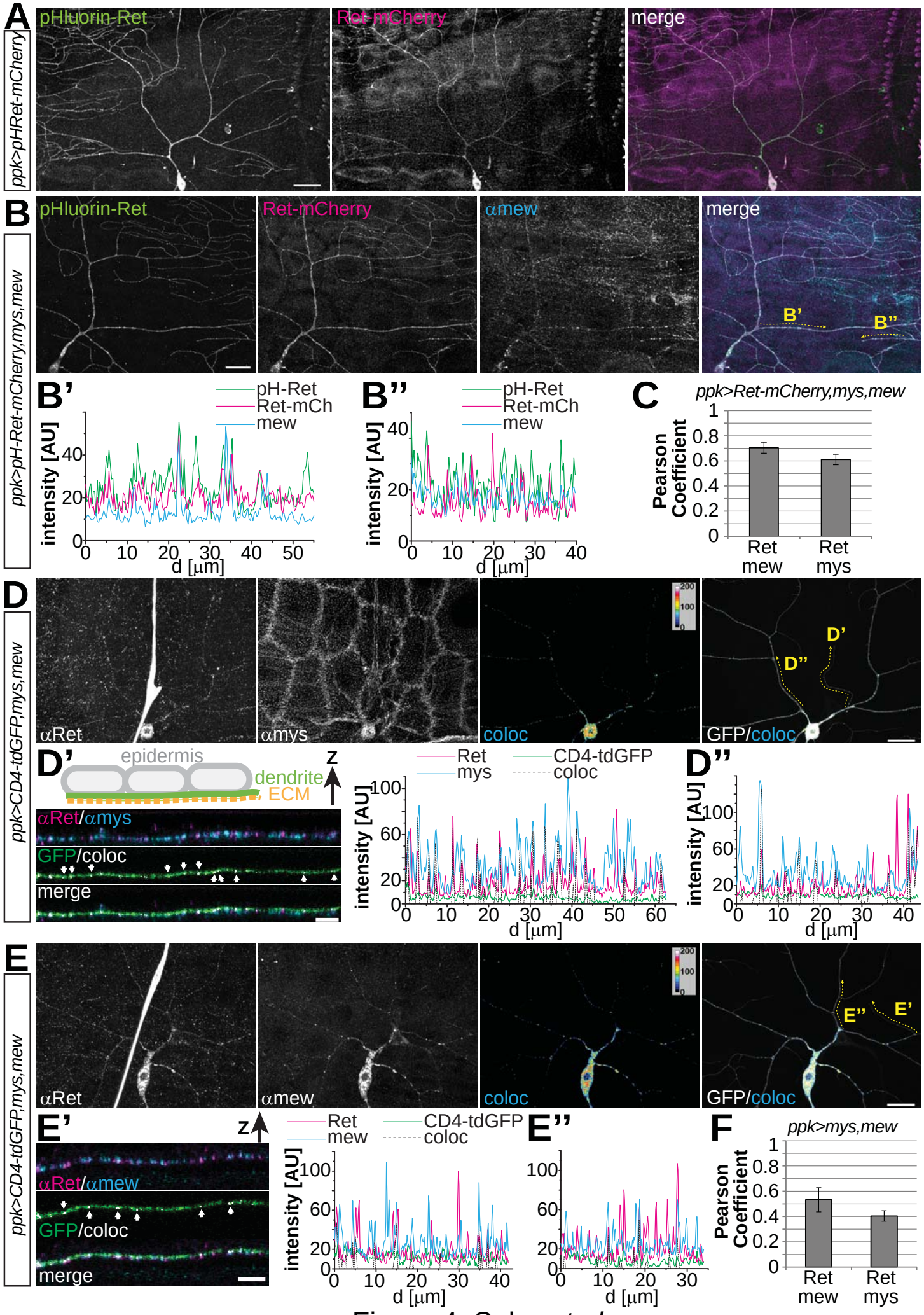


Figure 4, Soba *et al.*

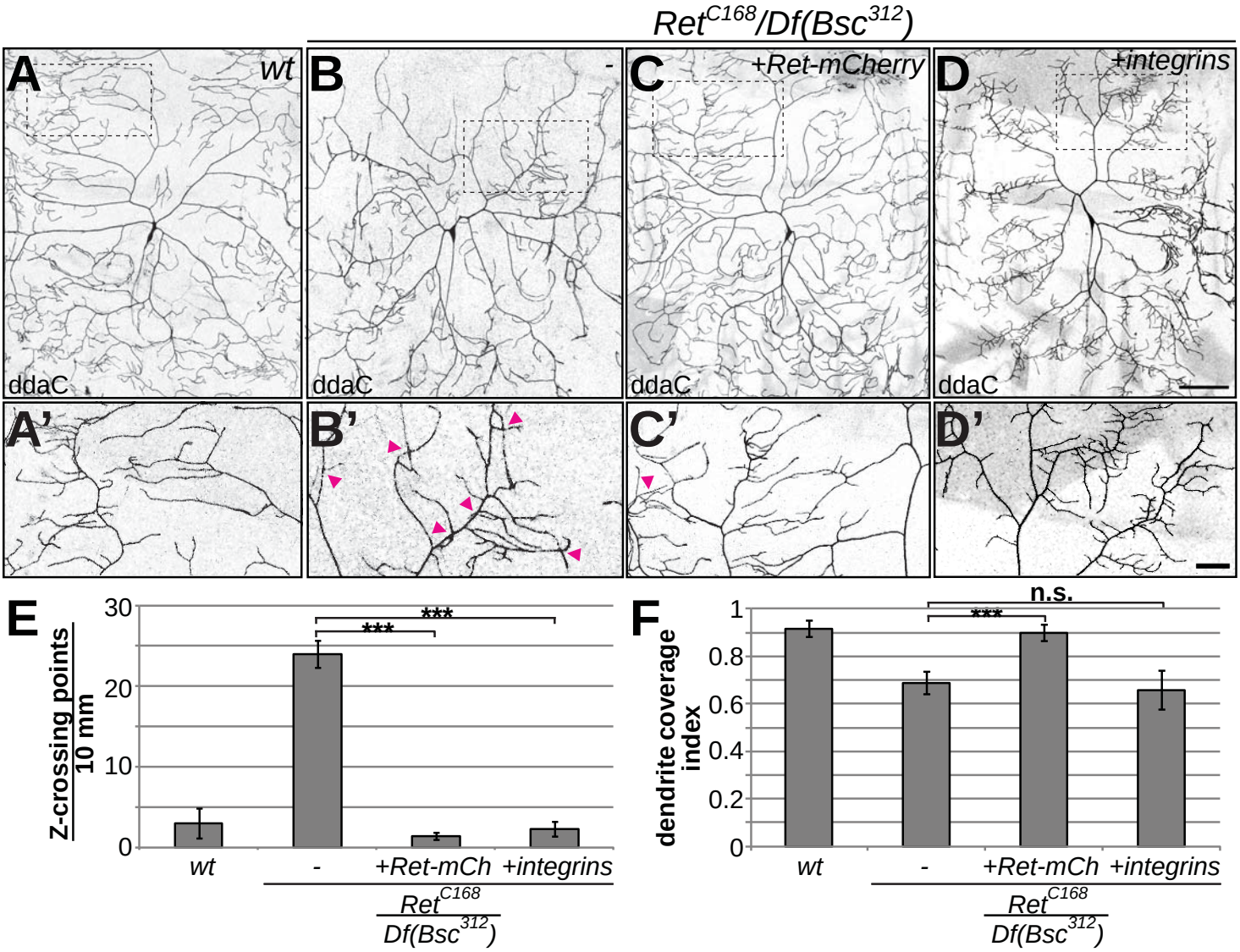


Figure 5, Soba *et al.*

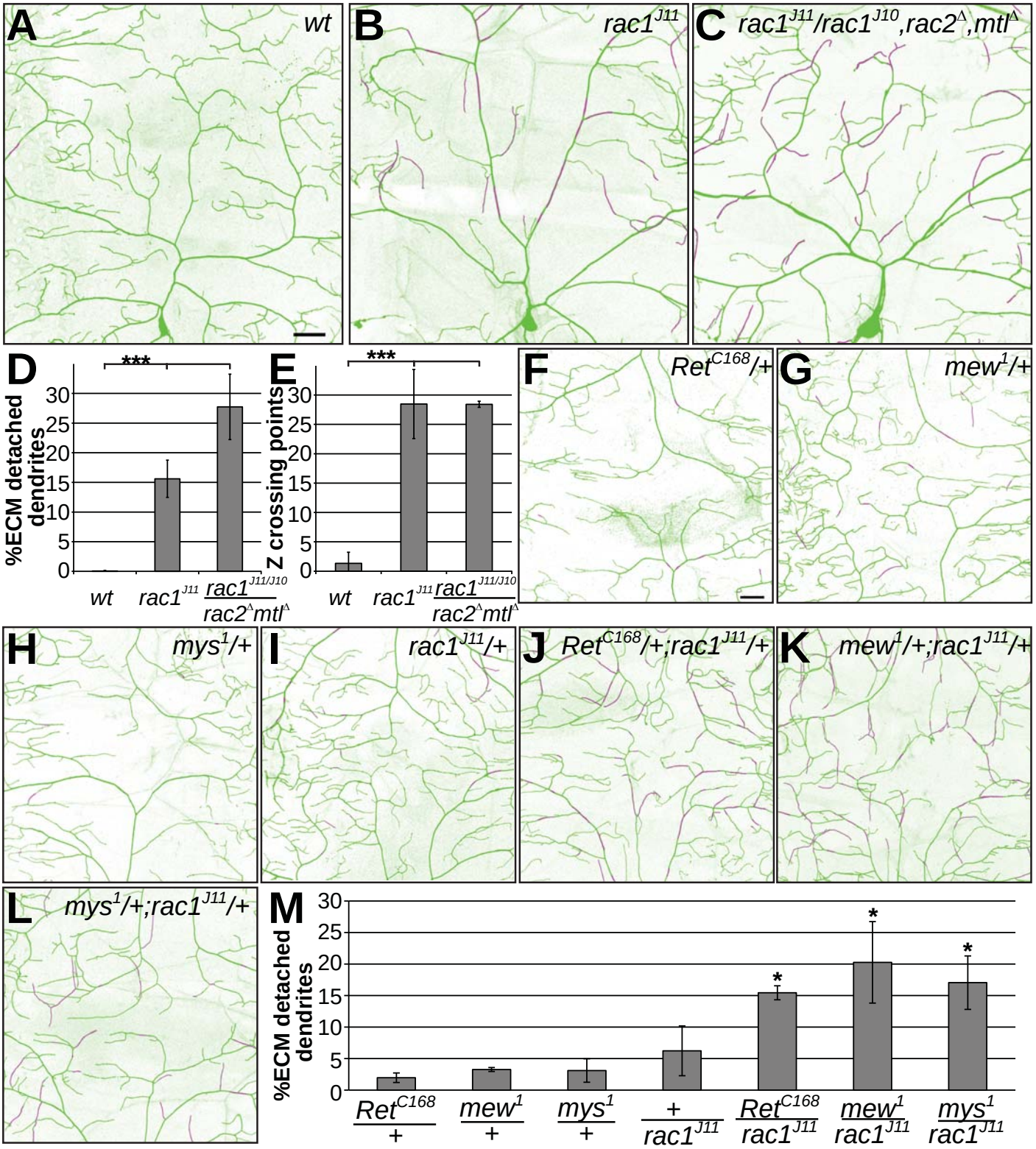
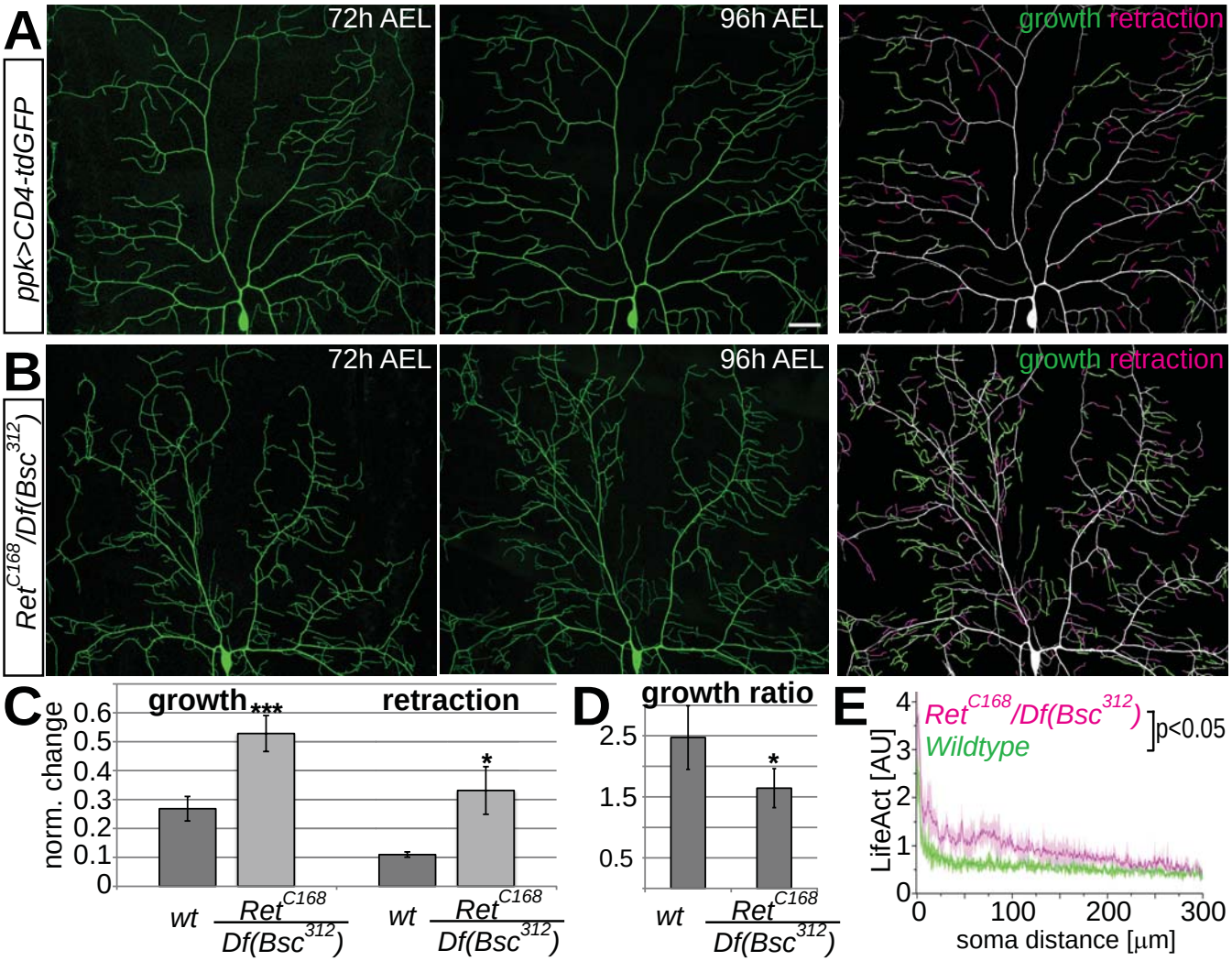


Figure 6, Soba *et al.*



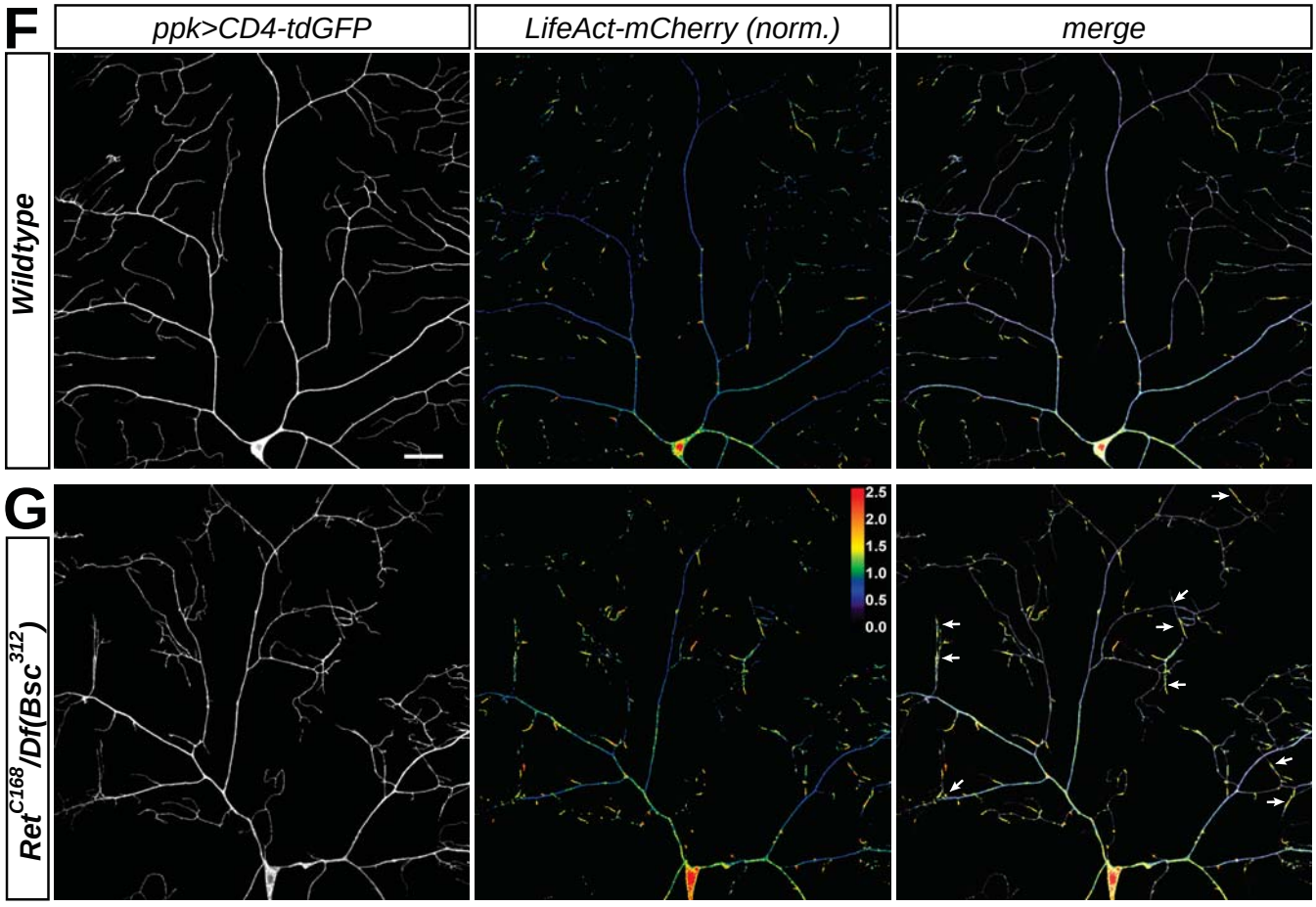


Figure 7, Soba *et al.*